Dynamics near the invariant manifolds after a Hamiltonian-Hopf bifurcation

E. Fontich[1,2] and A. Vieiro[1,2]

[1] Departament de Matemàtiques i Informàtica, Universitat de Barcelona (UB), Gran Via, 585, 08007 Barcelona, Spain
[2] Centre de Recerca Matemàtica (CRM), Campus Bellaterra, 08193 Bellaterra, Spain

October 12, 2022

Keywords: Hamiltonian dynamics, Hamiltonian-Hopf bifurcation, splitting of invariant manifolds, separatrix map

Abstract

We consider a one parameter family of 2-DOF Hamiltonian systems having an equilibrium point that undergoes a Hamiltonian-Hopf bifurcation. We briefly review the well-established normal form theory in this case. Then we focus on the invariant manifolds when there are homoclinic orbits to the complex-saddle equilibrium point, and we study the behavior of the splitting of the 2D invariant manifolds. The symmetries of the normal form are used to reduce the dynamics around the invariant manifolds to the dynamics of a family of area-preserving near-identity Poincaré maps that can be extended analytically to a suitable neighborhood of the separatrices. This allows, in particular, to use well-known results for area-preserving maps and derive an explicit upper bound of the splitting of separatrices for the Poincaré map. We illustrate the results in a concrete example. Different Poincaré sections are used to visualize the dynamics near the 2D invariant manifolds. Last section deals with the derivation of a separatrix map to study the chaotic dynamics near the 2D invariant manifolds.

1 Introduction

In this paper we study a one-parameter family of real analytic two degrees of freedom (2-DOF) Hamiltonian systems $H_\nu(\psi_1, \psi_2, J_1, J_2)$, $\nu \in \mathbb{R}$, having an equilibrium point (assumed to be at the origin for all parameter values) that undergoes a Hamiltonian-Hopf bifurcation [8, 29]. At this bifurcation the equilibrium point loses its linear stability as a consequence of a collision of the pure imaginary eigenvalues of the linearized vector field. Concretely, we deal with the following bifurcation scenario:

1. For $\nu > 0$ the matrix associated to the linear system at the origin has two pairs of purely imaginary eigenvalues: $\pm\omega_1\mathrm{i}$, $\pm\omega_2\mathrm{i}$, $\omega_1, \omega_2 > 0$.
2. At $\nu = 0$ the two pairs of eigenvalues meet in a double pair $\pm\omega\mathrm{i}$, $\omega > 0$.

3. For $\nu < 0$ the eigenvalues become a hyperbolic quartet $\pm\alpha \pm \omega \mathrm{i}\,,\ \alpha, \omega > 0$.

Then, for $\nu < 0$, the Hamiltonian system has an equilibrium point which is a complex-saddle point (CS from now on) and it possesses a 2D stable and a 2D unstable invariant manifold. We consider the case for which these invariant manifolds have a transversal intersection. We are interested in the geometry of the invariant manifolds and the dynamics around them.

More concretely, we deal with the 2-DOF Hamiltonian system

$$H(\psi_1, \psi_2, J_1, J_2) = \frac{J_1^2}{2} + a_2 J_1 J_2 + a_3 \frac{J_2^2}{2} - \cos\psi_1 - \epsilon \cos\psi_2, \tag{1}$$

defined on the symplectic manifold $(\mathbb{T}^2 \times \mathbb{R}^2, \Omega)$, where $\mathbb{T}^2 \simeq \mathbb{R}^2/(2\pi\mathbb{Z}^2)$ and $\Omega = d\psi_1 \wedge dJ_1 + d\psi_2 \wedge dJ_2$. For fixed values of a_2 and a_3, (1) is a one-parameter family of Hamiltonian systems.

The main motivation to consider Hamiltonian system (1) comes from the fact that it models the dynamics near a double resonance close to a totally elliptic equilibrium point of a 4D symplectic map. In this setting $|\epsilon|$ is related to the ratio of the orders of the two interacting resonances [20]. In Section 2 we summarize some of these ideas, adapted to the case considered here. It turns out that for values of a_2 and a_3 such that $d = a_3 - a_2^2 < 0$ there is a (negative) critical value $\epsilon = \epsilon_c$ for which the origin undergoes a Hamiltonian-Hopf bifurcation. Taking $\nu = \epsilon - \epsilon_c$ as the parameter, the family of Hamiltonian systems $H_\nu(\psi_1, \psi_2, J_1, J_2)$ shows up the bifurcation scenario described above.

The aim of this paper is to perform a numerical exploration of some of the properties of the system (1) when a CS point is born as a byproduct of the Hamiltonian-Hopf bifurcation. The paper is organized as follows.

In Section 2 we explain our motivation to study the model (1) and the role of the parameters involved. The numerical investigations start in Section 3 where we compute the 2D stable and unstable invariant manifolds of the complex-saddle point at the origin and their splitting for different values of ϵ.

Section 4 provides the theoretical framework to explain the results of Section 3. We summarize the main properties of the normal form (NF) analysis of the 2-DOF Hamiltonian-Hopf bifurcation and we derive an (exponentially small in ν) upper bound for the asymptotic behavior of the splitting of separatrices. The main result in Section 4.2 states that the splitting of the invariant manifolds can be reduced to a standard statement concerning the splitting of separatrices for an auxiliary 2D area-preserving map, and the corresponding upper bound easily follows from the results in [15].

In Section 5 we use a suitable Poincaré map with the aim of visualizing the dynamics near the separatrices and of providing some intuition about the topology of different orbits. In particular, we show that the numerical results about the splitting of separatrices included in Section 3 agree with the asymptotic behavior that the obtained upper bound describes.

Finally, Section 6 discusses the derivation of a return map adapted to this setting. We show that the dynamics around the invariant manifolds can be analyzed through a family of separatrix maps depending on the energy. To this end we consider the integrable system that provides the truncation of the NF given in Section 4. We fix a 3D Poincaré section in the 4D phase space and we investigate the time that orbits spend near the complex-saddle point before coming back to the 3D Poincaré section. Introducing suitable coordinates a 3D integrable return map is obtained. Such a map preserves the two (formal) first integrals provided by the NF. Next, the

effect of the splitting is added to obtain a non-integrable 3D separatrix map. When restricted to an energy level, the obtained return map gives a 2D return map and in fact, under some further simplifications we recover the usual Chirikov separatrix map, see [6, 37].

Four appendices complete this work. In Appendix A we give details on how the reduction to Sokolskii NF is carried out numerically. In Appendix B the set of parameters a_2, a_3 of the system (1) corresponding to bounded/unbounded invariant manifolds is investigated. In Appendix C we explore the possibility of using a different Poincaré section, given by the passage by the maximum distance from the complex-saddle (CS) point, that was used in [17] to study the Hamiltonian-Hopf bifurcation under a periodic forcing. Finally, Appendix D sumarizes the results of direct simulations of the return time to the suggested Poincaré sections.

The computations related to the splitting of the 2D invariant manifolds of the CS point require the systematic use of multi-precision arithmetic. The package PARI/GP [2] has been very useful to that end.

2 The model and double resonances of a 4D symplectic map

Let F be a real analytic 4D symplectic map with a totally elliptic doubly resonant equilibrium point at the origin. The (versal) unfolding of F (within the universe of symplectic maps) gives rise to a two parameter family of maps F_{δ_1,δ_2}, $\delta_1, \delta_2 \in \mathbb{R}$, such that $F_{0,0} = F$. The normal form reduction provides a 2-DOF Hamiltonian system describing the dynamics (at a formal level) of F_{δ_1,δ_2} in a neighborhood of the origin. Assume that for concrete values of δ_1 and δ_2, with $0 < |\delta_1| + |\delta_2| \ll 1$, the phase space exhibits a structure (expected to be similar to the Cartesian product of two pendula in the simplest situations) related to the double resonance. Then, as usual, the dynamics around such a doubly resonant structure can be studied by the lift of the Hamiltonian to the corresponding covering space. As shown in [20], after some rescaling of variables and assuming that the order of the two (primary) resonances is similar but different (quantitative estimates of the admissible orders are given in the mentioned reference), the dynamics near their intersection can be approximately described by the dynamics of system (1). We remark that the variables $J_1, J_2 \in \mathbb{R}$ and $\psi_1, \psi_2 \in \mathbb{S}^1$ are local action-angle variables in a suitable (q_1, q_2)-covering space (concretely, q_i are related to the multipliers of the elliptic point, which are assumed to be $2\pi p_i/q_i + \delta_i$, $p_i, q_i \in \mathbb{Z}$, $\delta_i \in \mathbb{R}$, $i = 1, 2$). The parameters a_2, a_3, ϵ in (1) are related to the unfolding parameters δ_1, δ_2 above. Moreover, the parameter ϵ is related to the difference of order of the two involved resonances. Thus, ϵ is a small parameter whenever the two resonances have different order. This fact simplifies the study of the model (1). Note that for $\epsilon = 0$ (and also for $a_2 = 0$) system (1) is (Liouville) integrable.

Let $d = a_3 - a_2^2$ so that the determinant of the matrix associated with the bilinear form that defines the quadratic part in the actions (J_1, J_2) of (1) is $d/4$. We assume, without loss of generality, that $\epsilon d > 0$ (consider $\epsilon \mapsto -\epsilon$ and $\psi_2 \mapsto \psi_2 - \pi$ otherwise). The Hamiltonian flow (1) has four equilibria: $p_1 = (0, 0, 0, 0)$, $p_2 = (\pi, 0, 0, 0)$, $p_3 = (0, \pi, 0, 0)$ and $p_4 = (\pi, \pi, 0, 0)$. For $|\epsilon| \ll 1$ the point p_1 is totally elliptic, p_2 is hyperbolic-elliptic, p_3 is elliptic-hyperbolic and p_4 is hyperbolic-hyperbolic.

Remark 2.1. The (non-symplectic) change of coordinates $\tilde{J}_1 = J_1 + a_2 J_2$, $\tilde{J}_2 = a_2 J_1 + a_3 J_2$, $\tilde{\psi_1} = \psi_1$, $\tilde{\psi_2} = \psi_2$ reduces (1) to the so-called two-pendulum system $\ddot{\psi}_1 = A \sin\psi_1 + B \sin\psi_2$, $\ddot{\psi}_2 = C \sin\psi_1 + D \sin\psi_2$, being $A = 1$, $B = a_2\epsilon$, $C = a_2$ and $D = a_3\epsilon$ (see [12]). The corresponding stability analysis (in terms of the A, B, C, D parameters) was carried out in, for example, [26].

For larger values of $|\epsilon|$ the linear stability of the fixed points changes. We focus on p_1 and look for its possible transition from totally elliptic to CS. If X_H denotes the vector field associated to (1), then the characteristic polynomial of $DX_H(p_1)$ is $p(x) = x^4 + (1 + \epsilon a_3)x^2 + \epsilon d$. Hence the eigenvalues leave the imaginary axis if

$$\Delta = (1 + a_3\epsilon)^2 - 4d\epsilon < 0, \tag{2}$$

and, in this case, the point p_1 becomes a CS point. At $\Delta = 0$ there is a Krein collision of eigenvalues. Since we are assuming that $\epsilon d > 0$ the following holds:

- For $d > 0$, since $a_3 = d + a_2^2 \geq d > 0$, one has $\Delta \geq (1 + d\epsilon)^2 - 4d\epsilon = (1 - d\epsilon)^2 > 0$ and therefore the CS transition of p_1 never takes place because there is no Krein collision.
- If $d < 0$ (it requires $\epsilon < 0$), the point p_1 suffers a Krein collision when

$$\epsilon = \left(-(2a_3 - 4d) \pm \sqrt{(2a_3 - 4d)^2 - 4a_3^2} \right) / (2a_3^2). \tag{3}$$

  Note that in this case, (3) provides real values of ϵ.

3 Invariant manifolds and their splitting

As follows from (2), a collision of the eigenvalues at the equilibrium point p_1 at the origin takes place when $\Delta = 0$. This gives two negative critical values ϵ_1^c and ϵ_2^c. For $\epsilon \in (\epsilon_1^c, \epsilon_2^c)$ the origin is a CS point. In this section we start our study of system (1) by computing the invariant manifolds $W^{u/s}(0)$, for ϵ in the previous range, and describing the asymptotic behavior of their splitting along a homoclinic trajectory when ϵ approaches the critical value ϵ_2^c.

The equations of motion corresponding to (1) are

$$\begin{array}{ll} \dot{\psi_1} = & J_1 + a_2 J_2, \qquad \dot{J_1} = -\sin(\psi_1), \\ \dot{\psi_2} = & a_2 J_1 + a_3 J_2, \quad \dot{J_2} = -\epsilon \sin(\psi_2). \end{array} \tag{4}$$

The right-hand part of equations (4) define a vector field X on $\mathbb{T}^2 \times \mathbb{R}^2$. We denote by R_ψ and R_J the reversors $R_\psi(\psi_1, \psi_2, J_1, J_2) = (-\psi_1, -\psi_2, J_1, J_2)$ and $R_J(\psi_1, \psi_2, J_1, J_2) = (\psi_1, \psi_2, -J_1, -J_2)$. The vector field X satisfies

$$R(X(\psi_1, \psi_2, J_1, J_2)) = -X(R(\psi_1, \psi_2, J_1, J_2)), \tag{5}$$

where R stands for either R_ψ or R_J.

For numerical illustrations we integrate (4) with

$$a_2 = 1/2 \quad \text{and} \quad a_3 = -3/4, \tag{6}$$

hence $\epsilon_1^c = -4$ and $\epsilon_2^c = -4/9$. Below we denote by ϵ_c the value ϵ_2^c, and we focus on the Hamiltonian-Hopf bifurcation taking place at this value of the parameter.

3.1 Numerical computation of the invariant manifolds

Consider $\epsilon \in (\epsilon_1^c, \epsilon_2^c)$ so that the origin is a CS point which lies on the 3D energy level $\{H = h\}$ with $h = -1 - \epsilon$. We recall that $\nu = \epsilon - \epsilon_c$ where $\epsilon_c = \epsilon_2^c$. Assume that there is a primary

intersection of the 2-dimensional invariant manifolds $W^u(0)$ and $W^s(0)$ such that the extension of the invariant manifolds up to this intersection is contained within an $\mathcal{O}(\sqrt{\nu})$-neighborhood of the origin. This happens under a suitable condition on a coefficient of degree four of the normal form of the Hamiltonian, see Section 4.1. In particular, such a condition is fulfilled for the parameters (6), see also Appendix B.

In such a case, the homoclinic set $W^u(0) \cap W^s(0) \subset \{H = h\}$ is generically 1D. From the R_ψ-reversibility relation (5) it follows that if $(\psi_1, \psi_2, J_1, J_2) \in W^u(0)$ then $(-\psi_1, -\psi_2, J_1, J_2) \in W^s(0)$. This suggests to consider $\Sigma = \{\psi_1 = 0, \psi_2 = 0\}$ and to look for homoclinic points in Σ. Generically $\{H = h\} \cap \Sigma \subset \mathbb{R}^4$ is a 1D submanifold and the points in the intersection $W^u(0) \cap \Sigma$ are homoclinic points. We compute below a homoclinic point $p_h \in \Sigma$ with $J_1 > 0$, see Fig. 1. The corresponding homoclinic orbit will be denoted as $\gamma(t)$. The R_J-reversibility implies that if $(0, 0, J_1, J_2) \in W^u(0) \cap \Sigma$ then $(0, 0, -J_1, -J_2) \in W^s(0) \cap \Sigma$, hence one obtains by symmetry another homoclinic trajectory.

The methodology to compute the homoclinic point p_h on Σ is quite standard. To compute the local invariant manifolds, we use the parameterization method, see [5, 25] and references therein. The following items summarize the main steps:

1. Computation of the local parameterization of the 2D unstable manifold by imposing the conjugation of the dynamics of the equation restricted to $W^u(0)$ to the linear dynamics on it, see [20]. If $s_1, s_2 \in \mathbb{R}$ denote the local parameters on $W^u(0)$, we represent the manifold as a series in the complex parameters $z_1 = s_1 + \mathrm{i}\, s_2$, $z_2 = \bar{z}_1$.

2. Truncation of the series to a suitable order N (depending on the parameters) and estimate the largest radius r_* (in the s_1, s_2 parameter space) such that the invariance equation is verified up to a tolerance `tol` inside the ball of radius r_* (`tol` and `Err` below are chosen according the required precision). The points on the circle of radius r_* can be parameterized by an angle $\beta \in [0, 2\pi)$.

3. Computation of β such that parameterizes a point on Σ. We proceed as follows:

   (a) We consider the discretization of β given by the equidistributed values $\{\beta_i\}_{i=1,\dots,1000}$. Each value of β_i gives an initial condition that can be numerically integrated (we use a Taylor method with a local error `Err`).

   (b) We consider the Poincaré section $\psi_2 = 0$ (see Remark 3.1 below). For each $i = 1, \dots, 1000$, we integrate the vector field taking as initial condition the point on the circle of radius r_* associated to the angle β_i. The integration is performed up to the Poincaré section $\psi_2 = 0$. Note that the Poincaré section $\psi_2 = 0$ might be crossed many times before we get the homoclinic point on Σ. We proceed as follows:

      i. We fix a small initial number `m` of crossings and we integrate the vector field up to finding the `m` crossing with $\psi_2 = 0$. In this way, for each i we obtain a point on $\psi_2 = 0$. Denote by $\psi_{1,i}$ the corresponding coordinate of this point.

      ii. If for a concrete i one has $\psi_{1,i}\psi_{1,i-1} < 0$ then we look for $\beta \in (\beta_{i-1}, \beta_i)$ such that $\psi_1 = 0$ (for simplicity, we use a secant method at this step). The parameter β obtained is hence related to a point $p_h \in \Sigma$. Otherwise, if there is no i verifying this last condition, we increase `m`.

Remark 3.1. For $a_3 < 0$ the hypersurface $\{\psi_2 = 0\}$ is transversal to the flow whenever $a_2 J_1 + a_3 J_2 \neq 0$, that is, the set of non-transversal points is given by `NT`$=\{J_2 = -a_2 J_1/a_3\}$. Then, if $h = H(0) = -1 - \epsilon$,

$$\{H = h\} \cap \texttt{NT} = \left\{ \frac{1}{2}\left(1 - \frac{a_2^2}{a_3}\right) J_1^2 - \cos(\psi_1) - \epsilon \cos(\psi_2) + 1 + \epsilon = 0 \right\},$$

and the intersection of the non-transversal points inside the origin energy level and $\psi_2 = 0$ is

$$\{H = h\} \cap \mathtt{NT} \cap \{\psi_2 = 0\} = \left\{ \frac{1}{2} \left(1 - \frac{a_2^2}{a_3} \right) J_1^2 - \cos(\psi_1) + 1 = 0 \right\},$$

which can be interpreted as the zero energy level of a pendulum Hamiltonian system, expressed in (ψ_1, J_1)-coordinates. This energy level contains the center point (stable equilibrium of the pendulum corresponding to the global minimum of the energy level set). In particular, $\{\psi_2 = 0\}$ defines a transversal Poincaré section outside the origin.

For $\epsilon = -0.5$ we have found that the primary homoclinic point at $W^u(0) \cap \Sigma$ with $J_1 > 0$ is $(J_1, J_2) \approx (1.3651453, -0.9100969)$, see Remark 3.2 below. The invariant manifolds of the origin together with the homoclinic trajectory $\gamma(t)$ are shown in Fig. 1. We have not displayed the homoclinic orbit near the origin, it simply spirals around in the corresponding plane governed by the linear approximation.

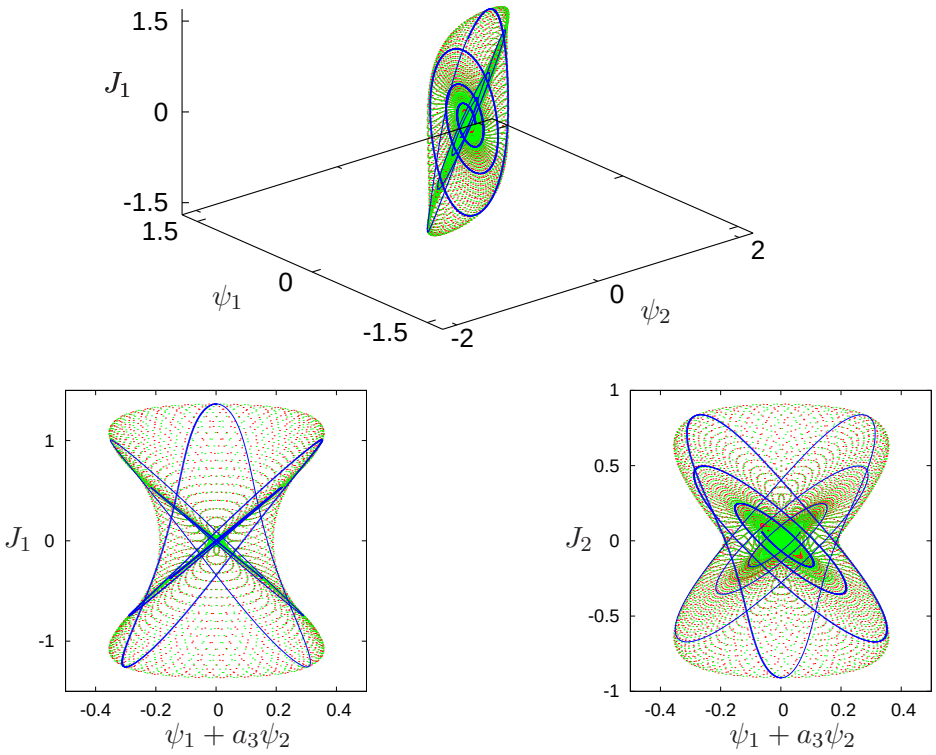

Figure 1: Top: We represent 3D projections of $W^u(0)$ (red) and $W^s(0)$ (green), corresponding to the flow of (4), for the parameters (6) and $\epsilon = -0.5$. See text for details. The homoclinic trajectory is shown in blue. Bottom left and right: Different projections showing a figure-eight shape of the manifolds.

Remark 3.2. One can numerically check that, for the range of ϵ used in the computations in this manuscript, there is only one primary homoclinic orbit that intersects Σ with $J_1 > 0$. We check this fact for $\epsilon = -0.5$ as follows. We propagate the initial conditions associated to the angles $\beta_k = 2\pi k/100$, $1 \leq k \leq 100$, on the circle of radius $r_* = 0.078572125$ until the 9th crossing with $\{\psi_2 = 0, J_1 > 0\}$ (computations are done with 200 digits, using a parameterization of order 80 and requiring precision 10^{-106} in the invariance equation). In Fig. 2 left we display the ranges of ψ_1 at the succesive crossings with $\{\psi_2 = 0, J_1 \geq 0\}$. In particular, we see that at the 5th crossing there are homoclinic points in $\Sigma \cap \{J_1 > 0\}$. The right plot in Fig. 2 shows that there is only one primary homoclinic point in $\Sigma \cap \{J_1 > 0\}$.

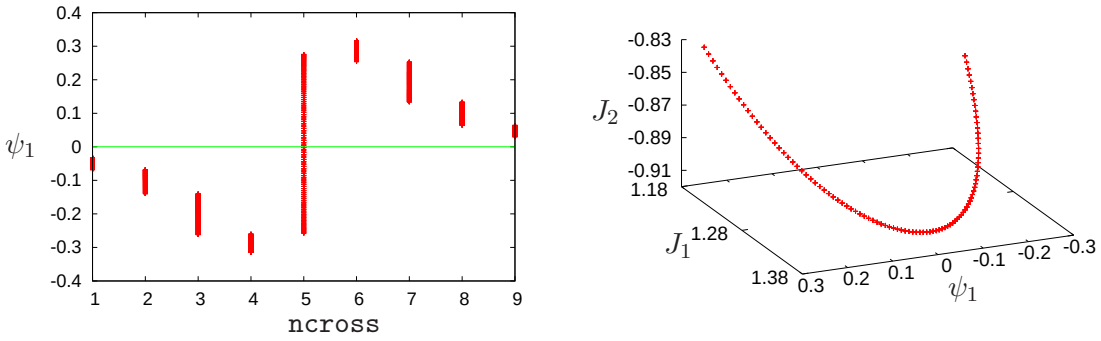

Figure 2: We consider $\epsilon = -0.5$. Left: We display the range of the variable ψ_1 in each of the $1 \leq \texttt{ncross} \leq 9$ first crossings with $\{\psi_2 = 0, J_1 > 0\}$. The line $\psi_1 = 0$ is shown for reference. Right: We display the propagated initial conditions at the 5th crossing, see text.

3.2 The splitting of the 2D invariant manifolds

It is well-known [39, 8, 24] that the Sokolskii NF of (1) provides, at least for small enough values of the parameter $\nu = \epsilon - \epsilon_c$, an integrable approximation of the dynamics around the CS point at the origin (in Section 4.1 we review the Hamiltonian-Hopf NF analysis). On the other hand, generically the vector field (4) is not integrable. In particular, for generic parameters one expects that the 2D invariant manifolds of the CS point do not coincide (see Fig. 1). The fact that the NF approximation is integrable suggests that their splitting is exponentially small in (some power of) ν according to the results in [31]. Below, we study the asymptotic behavior of the splitting angle of the 2D invariant manifolds for the parameters given in (6) and illustrate its exponentially small behavior in ν. We note that similar computations have been already performed in [18] for the Swift-Hohenberg equation.

To measure the splitting of the invariant manifolds (inside the energy level) of the CS point we compute an angle σ between tangent vectors to $W^u(0)$ and $W^s(0)$ at the homoclinic point. We denote by $T_p(M)$ the tangent space to a manifold M at the point p. Similarly as in [18, 20], we follow the next scheme to compute σ:

1. **Computation of the homoclinic trajectory.** Assume that the local parameterization of $W^u(0)$ is represented by a vector series $\mathcal{G}(s_1, s_2)$, $\mathcal{G} : \mathbb{R}^2 \to \mathbb{R}^4$. In the last section we explained how to obtain parameters (s_1^h, s_2^h) (on some circle of radius r_* around 0) such that $X_h^0 = (\psi_1^{h,0}, \psi_2^{h,0}, J_1^{h,0}, J_2^{h,0}) = \mathcal{G}(s_1^h, s_2^h)$ satisfies

$$\phi_{t=t_h}(X_h^0) \in \Sigma,$$

   where ϕ denotes the flow associated with (4) and t_h is the corresponding time to get the plane Σ.

2. **Computation of a basis of $T_{X_h^0}(W^u_{loc}(0))$.** A tangent vector to $W^u(0)$ at X_h^0 can be obtained, for example, by taking $v_t^0 = \frac{\partial \mathcal{G}}{\partial s_1}(s_1^h, s_2^h)$. By construction v_t^0 is not in the direction of the vector field $v_{\texttt{vf}}^0$. The vectors v_t^0 and $v_{\texttt{vf}}^0$ form a basis of $T_{X_h^0}(W^u_{loc}(0))$.

3. **Transportation of the vectors to Σ.** Integrating the variational equations along the homoclinic trajectory we transport v_t^0 to the section Σ. Denote by v_t^Σ the transported

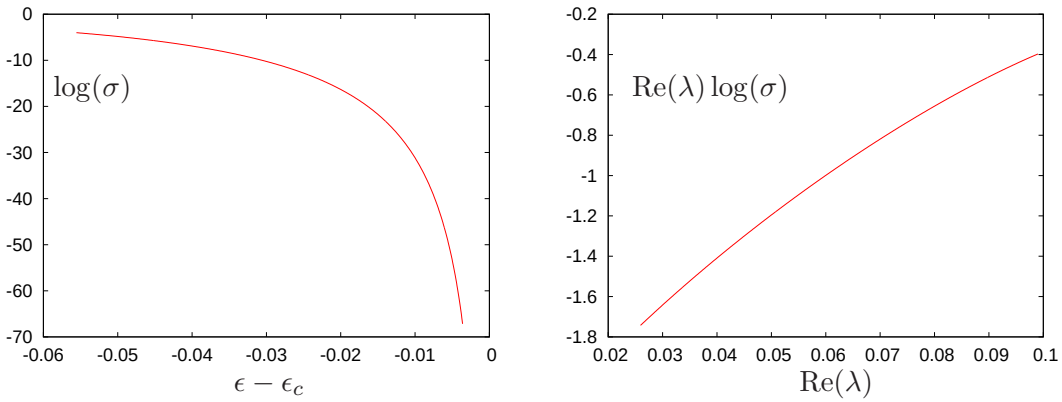

Figure 3: Angle σ for model (1) with parameters (6). Left: $\log(\sigma)$ as a function of $\epsilon - \epsilon_c$. Right: $\mathrm{Re}(\lambda)\log(\sigma)$ as a function of $\mathrm{Re}(\lambda)$, where $\lambda, \bar{\lambda}$ are the eigenvalues corresponding to $W^u(0)$.

vector. This vector together with the vector $v^{\Sigma}_{\mathtt{vf}}$, giving the direction of the vector field at the homoclinic point $h \in \Sigma$, form a basis of $T_h(W^u(0))$.

4. **Computation of σ.** We consider w_1 to be a unit normal vector to $v^{\Sigma}_{\mathtt{vf}}$ within $T_h(W^u(0))$. The reversibility R_J, see (5), allows us to easily compute a vector $w_2 \in T_h(W^s(0))$ orthonormal to $v^{\Sigma}_{\mathtt{vf}}$. We define σ to be the angle between w_1 and w_2.

To provide a concrete illustration we consider again the parameters in (6). We recall that $\epsilon_c = -4/9$. The results from the numerical computations are shown in Fig. 3. As expected, σ behaves asymptotically as an exponentially small quantity in $\nu = \epsilon - \epsilon_c$. Section 4.2 is devoted to derive a formula describing the asymptotic behavior of $\sigma(\nu)$ reflected in the figure.

3.3 The width of the analyticity strip of the homoclinic trajectory

It is well-known that for 1-DOF Hamiltonian systems having a homoclinic orbit $\gamma(t)$, the energy level restriction provides a 1D differential equation from which one can obtain (estimates of) the position of the complex singularities of γ as a function of complex time, see for example [36]. Moreover, in this 1-DOF setting one can prove that the singularity of the homoclinic trajectory exists and it is located at a finite distance from the real axis of t, see [14]. Note that here it plays a key role that the extension of the homoclinic trajectory to the complex plane defines an analytic function with an imaginary period and the existence of the singularity follows from Liouville's theorem.

However, for 2-DOF systems as the system (1), there is no systematic way to compute the position of the singularities of $\gamma(t)$. Moreover, for homoclinic trajectories $\gamma(t)$ to complex-saddle points the extension to $t \in \mathbb{C}$ is no longer periodic and conditions that guarantee the existence of the singularity are not known [13] although, as far as we are aware, there are no examples of entire homoclinic trajectories.

Here we investigate the width of the analyticity strip of the homoclinic trajectory $\gamma(t)$ through the homoclinic point $p_h \in \Sigma$ of the Hamiltonian system (1). We are interested in the closest (visible from the real time axis) singularity τ_0 of $\gamma(t)$. Our motivation is the following. The position of τ_0 can determine the width of the analyticity strip of $\gamma(t)$ when studying the splitting of the

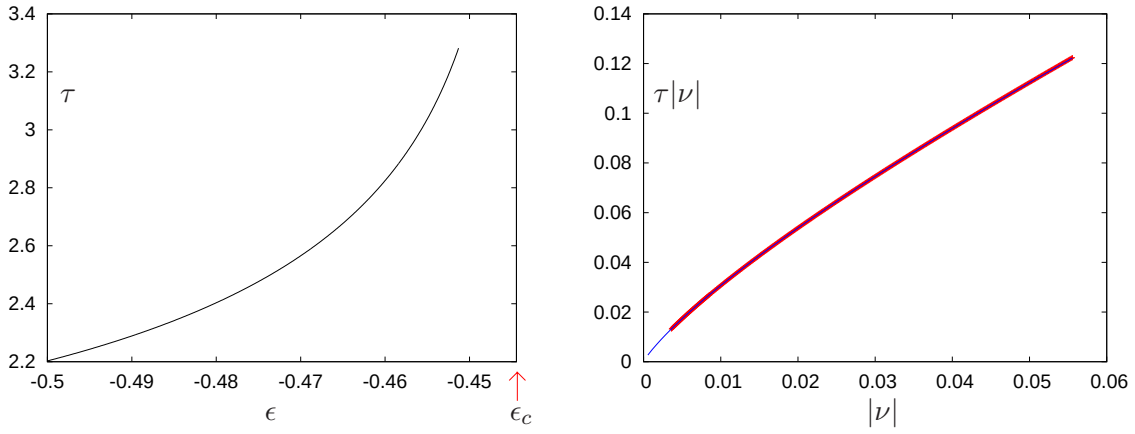

Figure 4: Values of τ corresponding to the closest singularity of the form $t = \tau \mathrm{i}$ to the real time axis of the homoclinic trajectory of the vector field generated by the Hamiltonian (1). Left: τ as a function of ϵ. Right: $\tau|\nu|$ as a function of $|\nu|$. The thin line represents the fit of the form $f(x) = ax\log(x) + bx + cx^2\log(x) + dx^2$, according to (7).

invariant manifolds under a periodic forcing of the original 2-DOF system. A periodic forcing in a similar, but more degenerate, situation was studied in [16, 17] where the quasi-periodicity of the splitting was analyzed. Note, however, that there the unperturbed (integrable) situation was a 2-DOF system having a 2D homoclinic manifold. Here, the unperturbed system is non-integrable and has a homoclinic orbit $\gamma(t)$. The splitting in the tangent and normal directions to that homoclinic orbit under the effect of periodic forcing and the role of the singularity τ_0 of $\gamma(t)$ are important questions that we aim to investigate in future works.

Below, we proceed with a numerical direct investigation. Inspired by similar (1-DOF) settings where the reversibility of the Hamiltonian system like (5) implies the existence of singularities in the purely imaginary time path we take the homoclinic point $p_h \in \Sigma$ as initial condition and we integrate the vector field along such a time path. In the experiment, we detect the position of a singularity because the modulus of some of the complex variables ψ_1, ψ_2, J_1, J_2 tends to infinity (that is, either the values become larger than some threshold, or the time-step of integration becomes too small). The results are shown in Fig. 4 left. A numerical exploration taking different paths in the complex time space suggests that the singularity $\tau\mathrm{i}$ obtained is the closest to the real axis. This supports that the analyticity strip of the homoclinic solution $\gamma(t)$ extends up to $\tau\mathrm{i}$. On the other hand, as expected, the numerical computations indicate that τ goes to ∞ when $\epsilon \to \epsilon_c = -4/9$ or, equivalently, when $\nu = \epsilon - \epsilon_c \to 0$. A fit of the numerical data, performed for $|\nu| < 0.01$, shows that

$$\tau \approx -0.612572\log(-\nu) + 0.182037 + 1.16972\nu\log(-\nu) - 1.07143\nu, \tag{7}$$

as it is displayed in Fig. 4 right.

4 Analysis of the bifurcation and splitting of separatrices

In this section, following the ideas of [15], we derive an explicit (and generically optimal) upper bound of the splitting of the 2D invariant manifolds. Before we briefly review the Sokolskii NF for the 2-DOF Hamiltonian-Hopf bifurcation.

4.1 Normal form reduction and global structure of the invariant manifolds

The equilibrium point at the origin of the Hamiltonian family (1) undergoes a Hamiltonian-Hopf bifurcation at $\nu = \epsilon - \epsilon_c = 0$. The NF reduction of a given one-parameter family of (real analytic) Hamiltonian systems $H_\nu(\psi_1, \psi_2, J_1, J_2)$ having a Hamiltonian-Hopf bifurcation at the origin for $\nu = 0$ was described in [17]. In this section, we briefly summarize the procedure to obtain the NF for a general case and comment on some computational aspects of this reduction that will be used in Section 5 for Hamiltonian (1).

Let H_ν be a general family of Hamiltonians, expressed in action-angle variables. Denote by X_{H_ν} the corresponding Hamiltonian vector field, and assume that 0 is an equilibrium point. We assume that for $\nu > 0$ the differential matrix $DX_{H_\nu}(0)$ has two pairs of pure imaginary eigenvalues that, for $\nu = 0$, meet in a double pair $\pm i\omega$, $\omega > 0$, on the imaginary axis (Krein collision) and that they become a hyperbolic quartet $\pm\alpha \pm i\omega$, $\alpha, \omega > 0$, for $\nu < 0$. To reduce H_ν to the Sokolskii NF we follow the next steps.

(i) We consider the Taylor expansion of H_ν in $(\psi_1, \psi_2, J_1, J_2)$ and ν around 0. If $\mathbb{P}_k$ denotes the set of homogeneous polynomials of degree $k \in \mathbb{N}$ in $(\psi_1, \psi_2, J_1, J_2)$ variables, one can express H_ν as

$$H_\nu = \sum_{k\geq 2} \sum_{j\geq 0} \nu^j H_{k,j}, \qquad \text{where } H_{k,j} \in \mathbb{P}_k \text{ for all } j \geq 0.$$

(ii) We look for a linear (symplectic) change of coordinates $\mathcal{L}(\psi_1, \psi_2, J_1, J_2) = (x_1, x_2, y_1, y_2)$ that reduces the quadratic part $H_{2,0}$ of H_ν to Williamson canonical form [41, 1]. In case of two pairs of (double) pure imaginary eigenvalues the Williamson NF is

$$H_{2,0} = -\omega(x_2 y_1 - x_1 y_2) + \frac{1}{2}(x_1^2 + x_2^2).$$

An effective algorithm to compute $\mathcal{L}$ was described in [4].

(iii) We simplify the higher order terms of H_ν by proceeding inductively order by order. At each step we look for a near-the-identity change generated by the time-1 map of a homogeneous polynomial Hamiltonian G. When trying to remove as many monomials $H_{k,j}$ of H_ν as possible one has to look for G such that

$$H_{k,j} + \mathrm{ad}_{H_{2,0}}(G) \in \mathrm{Ker}\, \mathrm{ad}^\top_{H_{2,0}}. \tag{8}$$

In Appendix A we describe how to compute G numerically at each step in a systematic way.

(iv) The theoretical analysis of the homological equation (8) simplifies by introducing the so-called polar Sokolskii coordinates through the change of coordinates $(x_1, x_2, y_1, y_2) \mapsto (R, \Theta, r, \theta) \in \mathbb{R}^2 \times (\mathbb{R} \setminus \{0\}) \times \mathbb{S}^1$, defined by the relations

$$y_1 = r\cos(\theta), \qquad y_2 = r\sin(\theta), \qquad R = (x_1 y_1 + x_2 y_2)/r, \qquad \Theta = x_2 y_1 - x_1 y_2. \tag{9}$$

Note that $\Omega = dx_1 \wedge dy_1 + dx_2 \wedge dy_2 = dR \wedge dr + d\Theta \wedge d\theta$, hence the change of coordinates is symplectic. Using these coordinates the transpose linear system (with matrix $J(D^2 H_2)^\top$ where J is the symplectic matrix) simplifies and one obtains the following expression of the (formal) normalized Hamiltonian

$$\mathrm{NF}(H_\nu) = -\omega\Gamma_1 + \Gamma_2 + \sum_{\substack{k,l,j\geq 0 \\ k+l+j\geq 2}} a_{k,l,j}\, \Gamma_1^k\, \Gamma_3^l\, \nu^j, \tag{10}$$

where $\Gamma_1 = \Theta = x_2y_1 - x_1y_2$, $\Gamma_2 = (x_1^2 + x_2^2)/2$ and $\Gamma_3 = (y_1^2 + y_2^2)/2$.

(v) One has that Γ_1 is a first integral of the system generated by $\mathrm{NF}(H_\nu)$. Writing explicitly the lowest order terms of $\mathrm{NF}(H_\nu)$ we have

$$\begin{aligned}\mathrm{NF}(H_\nu) &= -\omega\Gamma_1 + \Gamma_2 + \nu(a_{1,0,1}\Gamma_1 + a_{0,1,1}\Gamma_3) + a_{2,0,0}\Gamma_1^2 + a_{1,1,0}\Gamma_1\Gamma_3 + a_{0,2,0}\Gamma_3^2 \\ &\quad +\mathcal{O}(\nu^2(\Gamma_1+\Gamma_3), \nu(\Gamma_1+\Gamma_3)^2, (\Gamma_1+\Gamma_3)^3). \end{aligned} \tag{11}$$

(vi) To have a complex-saddle point for $\nu < 0$ requires $a_{0,1,1} > 0$. The rescaling

$$\nu = -\delta^2, \qquad x_i = \delta^2\tilde{x}_i, \quad \omega y_i = \delta\tilde{y}_i, \quad i = 1, 2, \qquad \omega t = \tilde{t}, \tag{12}$$

reduces (11) to

$$\mathrm{NF}(H_\delta) = -\tilde{\Gamma}_1 + \delta\left(\tilde{\Gamma}_2 + a\tilde{\Gamma}_3 + \eta\tilde{\Gamma}_3^2\right) + \mathcal{O}(\delta^2), \tag{13}$$

where

$$a = -a_{0,1,1}/\omega^2 \qquad \text{and} \qquad \eta = a_{0,2,0}/\omega^4. \tag{14}$$

and $\tilde{\Gamma}_i$ are as the functions Γ_i in (10) but depending on the rescaled variables $\tilde{x}_1, \tilde{x}_2, \tilde{y}_1, \tilde{y}_2$, that is,

$$\Gamma_1 = \frac{\delta^3}{\omega}\tilde{\Gamma}_1, \quad \Gamma_2 = \delta^4\tilde{\Gamma}_2 \quad \text{and} \quad \Gamma_3 = \frac{\delta^2}{\omega^2}\tilde{\Gamma}_3.$$

The rescaling (12) is not symplectic but the transformed system is also Hamiltonian. For $\eta > 0$ the invariant manifolds $W^{u/s}(0)$ are bounded while for $\eta < 0$ they are unbounded.

Given $s \geq 2$ let $\hat{\phi}_s$ be the change of coordinates, constructed as above in (i)-(iv), that normalizes H_ν up to order s (considering a total order together in ν and $(\psi_1, \psi_2, J_1, J_2)$). Let $\mathrm{NF}_s(H)$ be the truncation of $\mathrm{NF}(H_\nu)$ to order $s \geq 2$. In particular, $\mathrm{NF}_4(H_\nu)$ and $H_\nu \circ \hat{\phi}_4$ differ in the non-normalized terms of the remainder of order higher than 4.

Remark 4.1. From (11) one checks that the linearization at the origin of system (1) has eigenvalues $\lambda = \pm i\omega \pm \sqrt{a_{0,1,1}}\sqrt{-\nu} + \mathcal{O}(\nu)$. Then, for $\nu < 0$, one has $\mathrm{Re}(\lambda) = \pm\omega\sqrt{-a}\sqrt{-\nu} + \mathcal{O}(\nu)$ and $\mathrm{Im}(\lambda) = \pm\omega + \mathcal{O}(\nu)$.

Remark 4.2. The reduction to a NF is achieved by means of successive changes of coordinates to normalize order by order the full Hamiltonian as detailed in step (iii) above. Each of the changes of the averaging procedure reduces the validity domain of the truncated NF. For a fixed perturbation parameter ν, there is an optimal order to which the truncation of the NF gives the largest validity domain. However, the optimal order depends discontinuously on ν. See [31].

To describe the geometry of $W^{u/s}(0)$ it is useful to work with the coordinates (9), now expressed in terms of the previous coordinates $\tilde{x}_i$ and $\tilde{y}_i$, $i = 1, 2$, introduced in (12). One has

$$\tilde{\Gamma}_1 = \tilde{\Theta}, \quad \tilde{\Gamma}_2 = \frac{1}{2}\left(\tilde{R}^2 + \frac{\tilde{\Theta}^2}{\tilde{r}^2}\right), \quad \text{and} \quad \tilde{\Gamma}_3 = \frac{\tilde{r}^2}{2},$$

where $\tilde{r} = \tilde{y}_1^2 + \tilde{y}_2^2$ and $\tilde{R} = R/\delta^2$. Then, ignoring $\mathcal{O}(\delta^2)$ terms, $W^{u/s}(0)$ are given by

$$\tilde{R}^2 + a\tilde{r}^2 + \frac{1}{2}\eta\tilde{r}^4 = 0,$$

which corresponds to the zero energy level of a Duffing Hamiltonian system. However, note that here $\tilde{R}$ is a position and $\tilde{r}$ is an action. Hence, the restriction of $W^{u/s}(0)$ to the symplectic plane

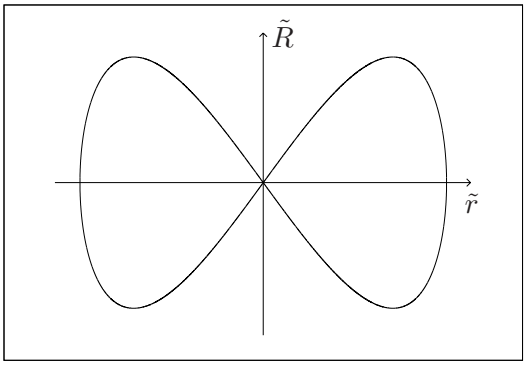

Figure 5: The figure-eight form of the manifolds $W^{u/s}(0)$ of $\mathrm{NF}_4(H_\nu)$ restricted to the $(\tilde{r}, \tilde{R})$-plane.

$(\tilde{R}, \tilde{r})$ describes, for $a < 0$ and $\eta > 0$, a figure-eight like the one shown in Fig. 5, but only the homoclinic loop with $r > 0$ makes sense in our framework. On the other hand, on the invariant manifolds $W^{u/s}(0)$ of the truncated system one has $\Theta = 0$ and $\dot{\theta} = 1$. Hence, the homoclinic solution is 2π-periodic in θ and the manifolds rotate around the origin in such a way that we may think that the left loop of the figure-eight in Fig. 5 corresponds to $\theta = \pi$.

As follows from item (v) above, any truncation $\mathrm{NF}_s(H)$, $s \geq 2$, of $\mathrm{NF}(H_\nu)$ becomes (Liouville) integrable and the pair $(\mathrm{NF}_s(H), \Gamma_1)$ of Poisson commuting real analytic Hamiltonian functions induces an energy-momentum map $M : \mathbb{R}^4 \to \mathbb{R}^2$. The action generated by Γ_1 is periodic but it is not free because it vanishes at the origin. The energy-momentum reduction becomes singular when $M(x_1, x_2, y_1, y_2) = (0, 0)$, that is, for the level set of the CS point. In the situation we are interested in, that is $\nu < 0$ and $\eta > 0$, one has that the fiber $M^{-1}(0, 0)$ is diffeomorphic to a pinched torus, that is, a 2D sphere with two different points identified. The other fibers of the energy-momentum map M are non-singular and, by the Liouville-Arnold theorem, they correspond to 2D tori. We refer to [8] for a complete discussion of the energy-momentum map in this setting.

The study of the homology group of M, taking closed loops around the singularity at $(0, 0)$, reveals non-trivial (Hamiltonian) monodromy of the fibration [10, 28, 44, 32]. This prevents from the existence of global action-angle coordinates in a neighborhood of the singular fiber $M^{-1}(0, 0)$ because they become multi-valued functions. This is reflected in Sokolkii coordinates in the singularity $r = 0$ of the R-coordinate in (9).

4.2 A theoretical formula for the splitting of separatrices

In this section we derive an explicit upper bound of the splitting of the 2D invariant manifolds of the origin for the 2-DOF Hamiltonian (1). The result follows from the simple idea of using the normal form (13) to approximate a suitable 2D area-preserving (isoenergetic) Poincaré map of (1). Then the upper bound is obtained from the results in [15]. It turns out that the upper bounds obtained in [15] are generic in the sense that they describe the asymptotic behavior of the splitting when the splitting function, which is a periodic function obtained as the difference of the values of a first integral on the unstable and the stable manifolds, has a non-zero first Fourier coefficient, see [23, 36, 37] for details. In Section 5 we show the agreement of a fit of the asymptotic behavior of the invariant manifolds computed numerically and shown in Fig. 3 with

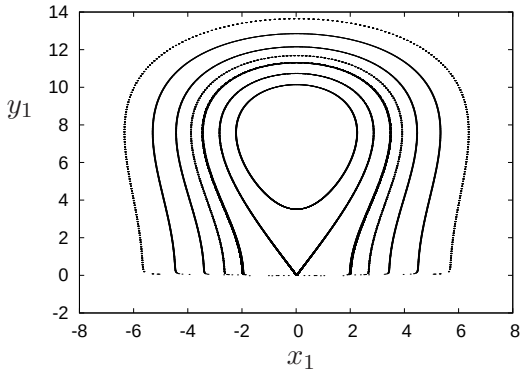

Figure 6: Phase portrait of the Poincaré map T_δ^0. On Σ we consider (x_1, y_1) as coordinates and we show the iterates of the Poincaré map obtained as a result of integrating the vector field corresponding to the Hamiltonian (13) ignoring the $\mathcal{O}(\delta^2)$ terms. The area-preserving map obtained is then integrable and possesses a homoclinic separatrix connection. The parameters taken for this figure are $a = -9/32$, $\eta = 5/1024$ and $\delta = 0.01$.

the theoretical expectations given by the upper bounds described here.

To avoid problems with the singularities associated with the polar (Sokolskii) coordinates we consider the Cartesian coordinates in which we have expressed the NF Hamiltonian (13). Concretely, we consider the non-integrable Hamiltonian $H_\nu \circ \hat{\phi}_4 \circ S_\delta$, where $\hat{\phi}_4$ is the change to normalize H_ν up to order four, S_δ refers to the scaling (12) and $\nu = -\delta^2$. For simplicity of notation we denote the previous Hamiltonian H_δ. We look at the dynamics within the zero energy level of H_δ where both $W^{u/s}(0)$ are contained. The discussion in Section 4.1 about the geometry of the invariant manifolds suggests to consider $\{\theta = 0\} \cap \{H_\delta = 0\}$ as a Poincaré section. This means to consider $\Sigma = (\{y_2 = 0, \dot{y}_2 > 0\} \setminus \{y_1 = 0\}) \cap \{H_\delta = 0\}$ as a Poincaré section and the corresponding family of (isoenergetic) Poincaré maps $T_\delta : \Sigma \to \Sigma$.

Let H_δ^0 be the integrable system obtained from H_δ ignoring the $\mathcal{O}(\delta^2)$ terms. For this system, a point $p \in \{y_2 = 0\} \cap W^{u/s}(0)$ is of the form $p = (x_1, 0, y_1, 0)$ because $H_\delta^0 = \tilde{\Gamma}_1 = 0$ on $W^{u/s}(0)$. The set of points at the intersection of the invariant manifolds $W^{u/s}(0)$ of H_δ^0 with $y_2 = 0$ are given by $x_1 = \pm y_1 \sqrt{-a - \eta y_1^2/2}$, hence they define a figure-eight like the one shown in Fig. 5 but on the (x_1, y_1) plane[1]. Consequently, the map T_δ^0 defined from H_δ^0 has a homoclinic loop (the upper loop of the figure-eight in the variables x_1, y_1, see Fig. 6). The phase portrait of the Poincaré map T_δ^0 for the values $a = -9/32$, $\eta = 5/1024$ and $\delta = 0.01$ is shown in Fig. 6. These values correspond to the parameters (6), see details in Section 5 below. Note the singularity at the axis $y_1 = 0$: only the origin belongs to Σ since $y_1 = y_2 = 0$ together with $H_\delta = 0$ implies $x_1 = x_2 = 0$. Indeed, any truncation of the series in (13) will show up a homoclinic loop (this is due to the fact that the system is integrable having H_δ^0 and $\tilde{\Gamma}_1$ as first integrals). If, on the other hand, we consider H_δ then the homoclinic loop generically splits (the system becomes generically non-integrable because $\tilde{\Gamma}_1$ is no longer a first integral). Consequently, this splitting is a beyond all orders phenomenon not detected in the series expansion of the Hamiltonian in δ.

The following proposition states some properties of the map T_δ^0 needed to describe the asymptotic behavior of the splitting of its separatrices.

Proposition 4.1. *The following properties for the Poincaré map T_δ^0 hold.*

[1] $\theta = 0$ implies $y_2 = 0$, hence $r = y_1$ and $R = x_1$.

1) T_δ^0 is an analytic area-preserving map in Σ.

2) The branches of the invariant manifolds $W^{u/s}(0)$ of T_δ^0 coincide along a curve. Such curve can be represented as the homoclinic connection $\gamma(t)$ of the vector field

$$\dot{R} = \delta\left(ar + \eta r^3\right), \qquad \dot{r} = -\delta R. \tag{15}$$

Its eigenvalues at the origin are

$$\mu = \pm 2\pi\sqrt{-a}\delta.$$

When considering $t \in \mathbb{C}$, the nearest singularities of $\gamma(t)$ to the real axis time are located at

$$t = \pm\frac{i\pi}{2\sqrt{-a}\delta}.$$

3) Let $\gamma(t) = (x_1(t), y_1(t))$. The homoclinic solution of the vector field satisfies

$$\gamma(t + 2\pi) = \Pi_\Sigma(\varphi_{t=2\pi}(p)),$$

where $p = (x_1(t), 0, y_1(t), 0)$, φ_t denotes the flow defined by H_δ^0 and Π_Σ denotes the projection onto Σ.

4) Let $p = (x_1, 0, y_1, 0) \in \Sigma$ such that $\bar{p} = \Pi_\Sigma(p) \in \gamma(t)$. Then

$$T_\delta^0(\bar{p}) = \hat{T}_\delta^0 \circ \hat{T}_\delta^0(\bar{p}),$$

where $\hat{T}_\delta^0 : \hat{\Sigma} \to \hat{\Sigma}$ is defined by $\hat{T}_\delta^0(\bar{p}) = \varphi_{t=\pi}(p)$, and $\hat{\Sigma} = \{y_2 = 0\} \cap \{H_\delta^0 = 0\}$.

Proof. By construction T_δ^0 is the Poincaré map associated with an analytic Hamiltonian vector field defined on an analytic Poincaré section Σ, hence 1) holds. To obtain the other properties it is enough to write down the equations of motion in Sokolskii coordinates. One has,

$$\dot{R} = \delta\left(-\frac{\Theta^2}{r^3} + ar + \eta r^3\right), \qquad \dot{r} = -\delta R, \qquad \dot{\Theta} = 0, \qquad \dot{\theta} = 1 - \delta\frac{\Theta}{r^2}. \tag{16}$$

Recall that Θ is a formal constant of motion and that $\Theta = 0$ on $W^{u/s}$. The reduction of the system to $W^{u/s}$ becomes 2π periodic in θ. The Poincaré section Σ becomes $\theta = 0$. The restriction of T_δ^0 to $W^{u/s}(0)$ coincides with the Poincaré stroboscopic map $\varphi_{\theta=2\pi}$ where φ denotes the flow of the vector field (16)) (the name stroboscopic comes from the fact that the variable θ can be considered as a new time of the system). In other words, the vector field (15) defines a vector field such that, given $q \in W^{u/s} \cap \Sigma$, T_δ^0 restricted to $W^{u/s}$ has the form

$$T_\delta^0(X) = \begin{pmatrix} \phi_{t=2\pi}(q_{Rr}) \\ \Theta \\ \theta \pmod{2\pi} \end{pmatrix} + \mathcal{O}(\delta^2),$$

where ϕ denotes the flow of (15) and q_{Rr} denotes the R and r components of the point q. This implies 3). Moreover, the eigenvalues of (15) at $(0, 0)$ are $\mu = \pm\delta\sqrt{-a}$. Let $\gamma(t)$ be the homoclinic orbit of the limit vector field (15). This is an analytic function in $t \in \mathbb{R}$ that can be extended for $t \in \mathbb{C}$ to the complex strip $|\mathrm{Im}\ t| \leq \mathrm{Im}\ \tau$, where $\tau \in \mathbb{C} \setminus \mathbb{R}$ denotes the nearest singularity to the real axis of time of $\gamma(t)$. The change of variables

$$u = \frac{\sqrt{\eta}}{a}R, \qquad v = \frac{\sqrt{\eta}}{\sqrt{-a}}r, \qquad \tilde{t} = \sqrt{-a}\,\delta\,t,$$

reduces (15) to the Duffing system

$$\dot{u} = v - v^3, \qquad \dot{v} = u,$$

with Hamiltonian $H = u^2/2 - v^2/2 + v^4/4$. On the homoclinic solution $\gamma(t)$ the following relation holds

$$\dot{v} = v\sqrt{1 - v^2/2}.$$

This permits to obtain an analytic expression of $\gamma(t)$ and get that the nearest singularities of γ to the real time axis are $\tau = \pm i\pi/2$. Undoing the rescaling we obtain 2).

Finally, 4) follows from the fact that $y_2 = 0$ if, and only if, either $\theta = 0$ or $\theta = \pi$. Note that the map $\hat{T}_\delta^0$ shows up a homoclinic figure-eight loop as depicted in Fig. 5. □

Our next goal is to apply the results in [15] to obtain an upper bound of the splitting of the separatrices of T_δ, sharp enough to describe the asymptotic behavior of the splitting. Note that, from the derivation of the NF Hamiltonian described previously, any Hamiltonian H_ν that undergoes a Hamiltonian-Hopf bifurcation is expected to have the same splitting as T_δ, hence the same asymptotic behavior.

First we need to rescale time to have the motion along the separatrices of T_δ approximated by the flow time-μ map of a limit vector field. It is enough to consider the limit vector field as considered in Prop. 4.1 and rescale time by $\sqrt{-a}\delta$. This implies that the imaginary part of the closest singularities move to Im $\tau = \pm\pi/2$.

In the following we assume that T_δ can be extended analytically to a neighborhood of $\{\gamma(t), |\text{Im } t| < \tau_0\}$, $0 < \tau_0 < \text{Im } \tau$. Under these hypotheses the following result was proven in [15]: for any $\eta > 0$ there exists δ^0 and $C > 0$ such that the distance between W^u and W^s measured at a point $p \in \gamma$ is bounded (uniformly in δ for $\delta < \delta^0$) by

$$C \exp\left(-2\pi(\text{Im } \tau_0 - \eta)/\mu\right). \tag{17}$$

We refer to [15, 36, 37, 14] for details and comments on this result.

A direct application of this result to the map T_δ fails to describe the asymptotic behavior of the splitting. The reason is that property 4) in Prop. 4.1 implies a half-period in the Fourier representation of the difference between the manifolds in a fundamental domain. Hence, we should consider $\mu/2$ instead μ in (17), see details in Remark 4.3 below. This is analogous to the situation taking place in the period-doubling bifurcation for area-preserving maps, see [19]. See also the related comments in [22, 21] about the splitting of the so-called "twisted" map [42].

As a conclusion the splitting σ of the invariant manifolds of T_δ is expected to behave asymptotically as

$$\sigma \sim A\delta^B \exp\left(\frac{-\pi}{\sqrt{-a}\delta}\right), \tag{18}$$

for some constants $A > 0$ and $B \in \mathbb{R}$. Equivalently, see Remark 4.1, the asymptotic behavior of σ is given by

$$\sigma \sim A\,|\text{Re } \lambda|^B \exp\left(\frac{-\pi\,|\text{Im } \lambda|}{|\text{Re } \lambda|}\right), \tag{19}$$

in terms of the eigenvalues of the original Hamiltonian system that undergoes the Hamiltonian-Hopf bifurcation.

Remark 4.3. Consider a near-the-identity family of area-preserving maps F_ϵ having a hyperbolic equilibrium point with eigenvalues $\lambda = 1 + \mathcal{O}(\epsilon)$. Let us recall the basic steps to obtain the upper bound (17), see [15].

1. One would like to construct a first integral (an energy) E to use it to measure the difference between the manifolds $W^{u/s}$. E is obtained from the NF at the hyperbolic point, which is convergent [30], and uniformly convergent with respect to the parameter ϵ [15].
2. The difference between the energy evaluated on each one of the manifolds $W^{u/s}$ turns out to be periodic with period $h = \log\lambda$. Then one bounds the coefficients of the Fourier expansion of the previous difference to obtain (17).

Consider now an area-preserving family of maps F_ϵ close to minus-the-identity map. Then, F_ϵ^2 is a near-the-identity family of maps which has a hyperbolic point. Assume that the dominant eigenvalue of F^2 is λ. In this situation, to derive a sharp upper bound able to describe the asymptotic behavior of the splitting, one should adapt the proof of (17). Consider $G_\epsilon = -F_\epsilon$. The NF at the hyperbolic point provides a first integral E of G_ϵ. The difference of the first integral evaluated on the invariant manifolds of G_ϵ gives a $(\log(\lambda)/2)$-periodic function. We note that the energy E is also a first integral of $G^2 = F^2$. Then, the splitting of the invariant manifolds of F^2 can be described also in terms of E, but it gives a $(\log(\lambda)/2)$-periodic function instead. If one performs the Fourier expansion in terms of this half-period and bounds the coefficients as in [15] one directly obtains a sharp upper bound that agrees with the asymptotic behavior given by (18).

As a final comment we note that the formula derived in [18] for the splitting is similar to (18), but has a factor $\pi/2$ in the exponential part instead of π as property 4) of Prop. 4.1 implies.

5 Visualizing the dynamics around the invariant manifolds

In this section we investigate the dynamics of the Hamiltonian system (1) through the reduction to a Poincaré section and, in particular, we check the asymptotic behavior of the splitting of $W^{u/s}(0)$ as $\nu = \epsilon - \epsilon_c \to 0$ from our numerical computations.

As a preliminary step we compute the changes of coordinates needed to reduce the Hamiltonian to the Sokolskii NF. To systematically determine the changes of coordinates we use the tools sketched in Section 4.1: the Burgoyne-Cushman algorithm [4] to put the quadratic part of H in the desired form and the Lie method to deal with the higher order terms (see Appendix A). For concreteness, we consider the values of a_2, a_3 in (6).

The linear (symplectic) change of coordinates $\mathcal{L}(\psi_1, \psi_2, J_1, J_2) = (x_1, x_2, y_1, y_2)$ defined by

$$x_1 = \frac{1}{2}\psi_1 - \frac{1}{3}\psi_2, \qquad x_2 = \frac{-1}{\sqrt{6}}J_1 - \frac{\sqrt{3}}{2\sqrt{2}}J_2, \qquad y_1 = \frac{5}{4}J_1 - \frac{9}{8}J_2, \qquad y_2 = \frac{3\sqrt{3}}{4\sqrt{2}}\psi_1 + \frac{5}{2\sqrt{6}}\psi_2, \quad (20)$$

reduces the quadratic part of the Hamiltonian (1) at the bifurcation value, that is, when $\epsilon = \epsilon_c = -4/9$, to $H_2 = -\omega(x_2y_1 - x_1y_2) + \frac{1}{2}(x_1^2 + x_2^2)$ with $\omega = \sqrt{2/3}$. Moreover, the change of variables generated by the flow of the Hamiltonian

$$\begin{aligned} G \;=\; & \nu\,(g_1\; x_1x_2 + g_2\; x_1y_1 + g_3\; x_2y_2 + g_4\; y_1y_2) \\ & + g_5\; x_1^3x_2 + g_6\; x_1^3y_1 + g_7\; x_1^2x_2y_2 + g_8\; x_1^2y_1y_2 + g_9\; x_1x_2^3 + g_{10}\; x_1x_2^2y_1 \\ & + g_{11}\; x_1x_2y_1^2 + g_{12}\; x_1x_2y_2^2 + g_{13}\; x_1y_1^3 + g_{14}\; x_1y_1y_2^2 + g_{15}\; x_2^3y_2 + g_{16}\; x_2^2y_1y_2 \\ & + g_{17}\; x_2y_1^2y_2 + g_{18}\; x_2y_2^3 + g_{19}\; y_1^3y_2 + g_{20}\; y_1y_2^3, \end{aligned} \quad (21)$$

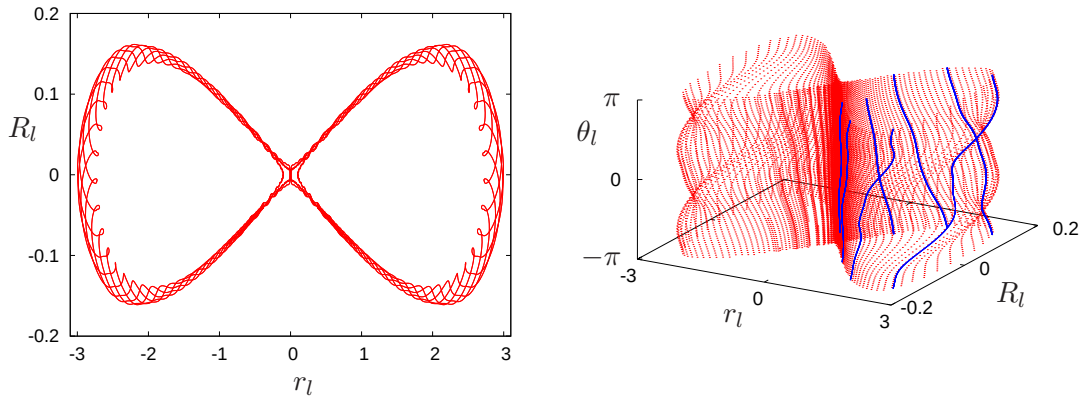

Figure 7: The invariant manifolds $W^{u/s}(0)$ shown in Fig. 1 are here represented in Sokolskii polar coordinates, see text for details. The left plot shows the projection onto the (r_l, R_l)-plane, compare with Fig. 5. The right plot displays the θ_l variable ranging in the vertical axis and, in blue, the homoclinic orbit also shown in Fig. 1.

where

$$g_1 = \frac{153\sqrt{3}}{256\sqrt{2}}, \quad g_2 = -\frac{9}{256}, \quad g_3 = -\frac{153}{256}, \quad g_4 = -\frac{3\sqrt{3}}{32\sqrt{2}}, \quad g_5 = -\frac{2713\sqrt{3}}{131072\sqrt{2}},$$
$$g_6 = \frac{20197}{393216}, \quad g_7 = -\frac{12397}{131072}, \quad g_8 = \frac{3143\sqrt{3}}{49152\sqrt{2}}, \quad g_9 = -\frac{2455\sqrt{3}}{131072\sqrt{2}}, \quad g_{10} = \frac{13171}{131072},$$
$$g_{11} = -\frac{2353\sqrt{3}}{49152\sqrt{2}}, \quad g_{12} = \frac{3713\sqrt{3}}{49152\sqrt{2}}, \quad g_{13} = \frac{395}{73728}, \quad g_{14} = \frac{1463}{73728}, \quad g_{15} = \frac{2455}{131072},$$
$$g_{16} = -\frac{893\sqrt{3}}{16384\sqrt{2}}, \quad g_{17} = -\frac{793}{73728}, \quad g_{18} = -\frac{517}{73728}, \quad g_{19} = -\frac{5\sqrt{3}}{9216\sqrt{2}}, \quad g_{20} = -\frac{25\sqrt{3}}{27648\sqrt{2}},$$

reduces H to the Sokolskii NF up to order 4. The corresponding coefficients in (11) are

$$a_{0,1,1} = \frac{3}{16}, \quad a_{1,0,1} = \frac{9\sqrt{3}}{32\sqrt{2}}, \quad a_{2,0,0} = -\frac{19}{4608}, \quad a_{1,1,0} = \frac{47\sqrt{2}}{1536\sqrt{3}}, \quad a_{0,2,0} = \frac{5}{2304}.$$

According to (14) one has $a = -9/32$ and $\eta = 5/1024$, then for $\nu = \epsilon - \epsilon_c < 0$ the invariant manifolds $W^{u/s}(0)$ are bounded. In Fig. 1 we displayed $W^{u/s}(0)$ for $\epsilon = -1/2$. Recall that in Section 4.1 we described the geometry of $W^{u/s}(0)$ in terms of the Sokolskii polar coordinates (9). In Fig. 7 we show $W^{u/s}(0)$ for $\epsilon = -1/2$ represented in the coordinates

$$(R_l, \Theta_l, r_l, \theta_l) = \mathcal{S} \circ \mathcal{L}(\psi_1, \psi_2, J_1, J_2), \tag{22}$$

that is, given by the composition of the linear change (20) with the change to Sokolskii polar coordinates (9), that is, without any normalization step. This change of coordinates is independent of ν.

5.1 The Poincaré map T_δ for the system H

The original system (1), for most of the parameters is non-integrable and the formal first integral Γ_1 is not preserved. This causes the splitting of separatrices which generates dynamical chaos.

Recall that the CS point of H is located at the energy level $H(0) = -1 - \epsilon$. Based on the previous considerations, here we use the section $\Sigma_l = \{\theta_l = 0\} \cap \{H = -1 - \epsilon\}$ to visualize the dynamics of (1). We denote the corresponding return map by T_δ by analogy to the return map introduced in Section 4.2 for H_δ. But note that the iterates of the return map $T_\delta : \Sigma_l \to \Sigma_l$ considered here are computed integrating (1) and applying the change of coordinates (22) to compute points with $\theta_l = 0$.

First, let us give some details on how we find the initial conditions to integrate equations (4). Given r_l, Θ_l, $r_l \neq 0$, we look for initial conditions on Σ_l with $R_l = 0$. We compute $(\psi_1, \psi_2, J_1, J_2) = \mathcal{L}^{-1} \circ \mathcal{S}^{-1}(0, \Theta_l, r_l, 0)$ using (22). It follows from (9) that $\mathcal{S}^{-1}(0, \Theta_l, r_l, 0) = (0, \Theta_l/r_l, r_l, 0)$. Using (20) one obtains

$$(\psi_1, \psi_2, J_1, J_2) = \left(0, 0, \frac{r_l}{2} - \frac{3\sqrt{3}}{4\sqrt{2}}\frac{\Theta_l}{r_l}, -\frac{r_l}{3} - \frac{5}{2\sqrt{6}}\frac{\Theta_l}{r_l}\right). \tag{23}$$

Imposing the point (23) to be in the energy level $h = H(0) = -1 - \epsilon$ leads to $g(r_l, \Theta_l) = 0$, where

$$g(r_l, \Theta_l) = \frac{1}{2}\left(\frac{r_l}{2} - \frac{3\sqrt{3}}{4\sqrt{2}}\frac{\Theta_l}{r_l}\right)\left[\left(\frac{r_l}{2} - \frac{3\sqrt{3}}{4\sqrt{2}}\frac{\Theta_l}{r_l}\right) - \left(\frac{r_l}{3} + \frac{5}{2\sqrt{6}}\frac{\Theta_l}{r_l}\right)\right] - \frac{3}{8}\left(\frac{r_l}{3} + \frac{5}{2\sqrt{6}}\frac{\Theta_l}{r_l}\right)^2.$$

One has $2r_l^2 g(r_l, \Theta_l) = -kr_l^2\Theta_l + \Theta_l^2$, being $k = 2\sqrt{2}/\sqrt{3}$, which vanishes if $\Theta_l = 0$ or $\Theta_l = kr_l^2$. Therefore we iterate points with $R_l = \Theta_l = \theta_l = 0$ and $r_l > 0$ to explore the phase space of T_δ. On the other hand, choosing $\Theta_l = kr_l^2$ allows us to explore solutions with different values of Θ_l that lie in the same energy level, however for values of $r_l \approx 0$ the dynamics resembles the previous one and for larger values of r_l most of the points escape.

Using the coordinates (22) one can compute the intersection of the invariant manifolds with the section $\{\theta_l = 0\}$. This is shown in Fig. 8 top together with iterates of the map T_δ. The figure also highlights the chaotic region around the invariant manifolds (that can be clearly observed near the origin as shown in the bottom left plot).

We remark that Σ_l is not a global transversal section. This contrasts with what happens when considering any truncation of the NF of H_ν where the singularity $y_1 = 0$ inside the energy level of the CS reduces to the origin, see comments in Section 4.2. However, H does not preserve Γ_1 and orbits can approach $r_l = 0$ where the corresponding Poincaré map is not well-defined. In Fig. 8 bottom left we magnify the phase portrait near the CS point. Finally, in Fig. 8 bottom right we see the transversal splitting of the invariant manifolds. Note that this region is far from $r = 0$ and the Poincaré map is well-defined on it. The observed splitting corresponds to the splitting of an area-preserving map as explained in Section 4.2. The existence of transverse homoclinic trajectories to the complex unstable point lead to the existence of horseshoes and chaos [9].

The expansion of the term $\cos(\psi_1) + \epsilon\cos(\psi_2)$ of H around the origin shows that the quadratic terms (in J_1, J_2) of the Hamiltonian (1) form a non-degenerate quadratic form that, for a fix energy level, defines a 4D imaginary hyperboloid homotopic to $\mathbb{R}^3 \times \mathbb{S}^1$. For the energy level of the origin, the slice $\theta = 0 \pmod{\pi}$ of the 4D hyperboloid is the conical 3D surface represented in Fig. 9.

Finally, we consider some iterates of the homoclinic point at $(R_l, r_l) \approx (2.730290, 0)$, see Fig. 8 bottom right. The first two iterates are $(1.967828, 1.584435 \times 10^{-1})$ and $(1.029221, 9.853949 \times$

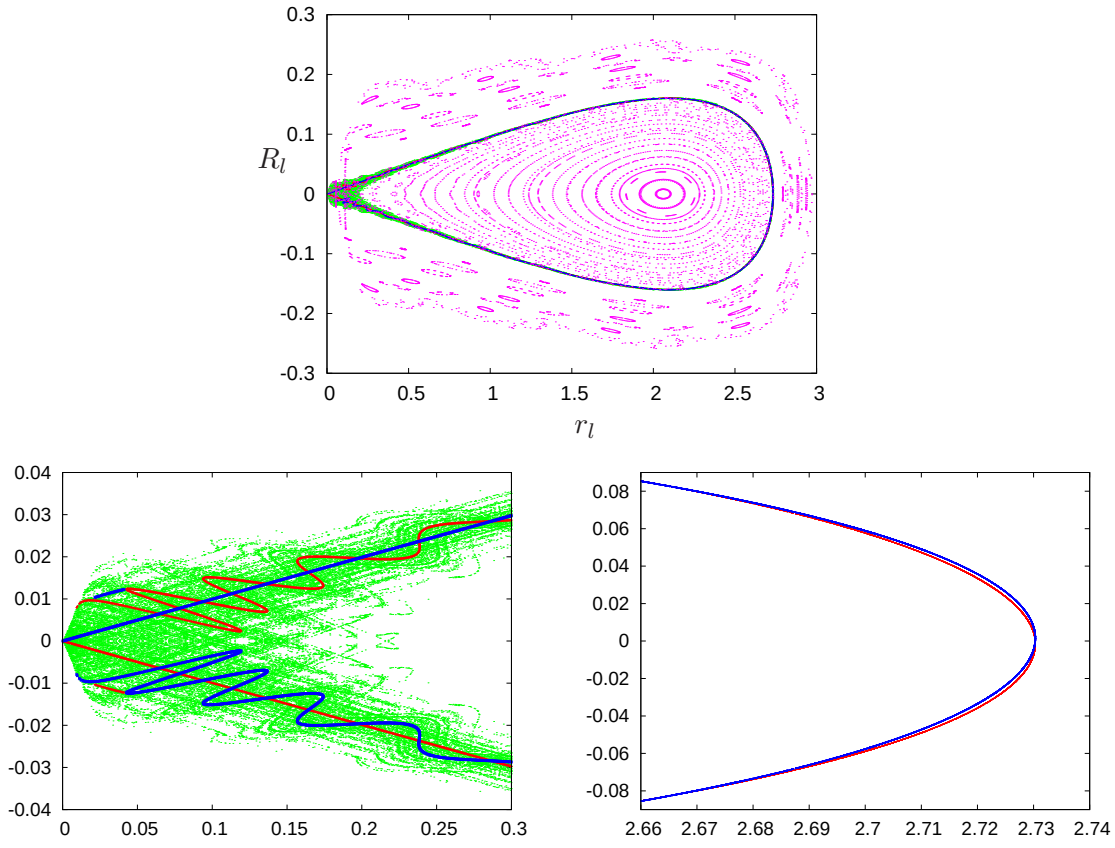

Figure 8: For the values in (6) and $\epsilon = -0.5$, we show the intersection of the invariant manifolds $W^{u/s}(0)$ with $\{\theta_l = 0\}$. In the top plot, iterates of the map T_δ are also represented and the chaotic zone along the invariant manifolds is highlighted. The bottom left plot is a magnification of the previous one to clearly observe the neighborhood of the origin. The bottom right plot is a magnification of the intersection of the invariant manifolds where we observe the splitting of separatrices far from the origin, where T_δ is well-defined as an area-preserving map. In all plots the variable r_l ranges in the vertical axis and the variable R_l in the horizontal one.

10^{-2}), respectively. In Fig. 10 we represent these first two iterates and we show the graph of the unstable manifold with respect to the stable manifold (in suitable coordinates so that the stable manifold becomes horizontal). The plot shows that the splitting function, that represents the unstable manifold with respect to the stable one (in a fundamental domain, that is, between consecutive iterates of the homoclinic point), has the second order harmonic as the dominant one. In particular, four homoclinic orbits coexist in a fundamental domain of the invariant manifolds for the Poincaré map T_δ.

5.2 A numerical check of the splitting behavior

Let us consider again the values of the splitting angle σ computed in Section 3.2 and shown in Fig. 3. We recall that in Section 3.2 we computed homoclinic points $p_h \in \{\psi_1 = 0\} \cap \{\psi_2 = 0\}$, then by the change (20) those points are such that $x_1 = y_2 = 0$, $\dot{y}_2 = -\omega y_1 < 0$, hence they are in the transversal section considered in Section 4.2. Then, according to the theory we expect that the splitting σ, that is the angle between $W^{u,s}$ of the Poincaré map T_δ at the homoclinic

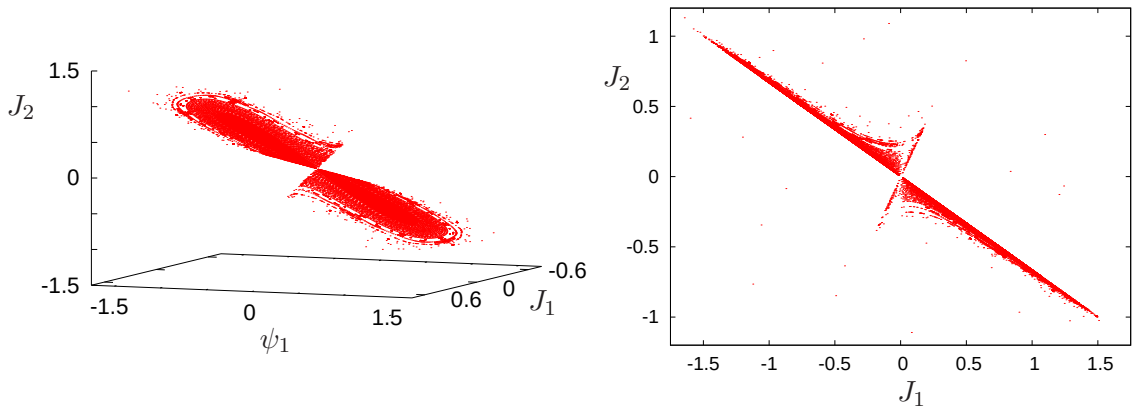

Figure 9: The left plot shows the 3D cone section obtained as intersection of the 4D hyperboloid with $\theta_l = 0 \pmod{\pi}$. We have used $\epsilon = -0.475$ and we represent the coordinates (ψ_1, J_1, J_2). The right plot is a projection onto (J_1, J_2) of the left one.

point, behaves asymptotically as

$$\sigma \sim \tilde{A} |\mathrm{Re}\,\lambda|^B \exp\left(\frac{-C}{|\mathrm{Re}\,\lambda|}\right), \tag{24}$$

where $C = \pi|\omega|$. Recall that $\delta = \sqrt{-\nu}$, $\nu = \epsilon - \epsilon_c < 0$. For the values (6), $\epsilon_c = -4/9$, and one checks that

$$\mathrm{Re}\,\lambda = \pm\frac{\sqrt{3}}{4}\sqrt{-\nu} + \mathcal{O}(\nu), \qquad \mathrm{Im}\,\lambda = \pm\sqrt{\frac{2}{3}} + \mathcal{O}(\nu),$$

according to Remark 4.1 and the previously derived value of $a = -9/32$. In particular, one expects $C = \sqrt{2}\pi/\sqrt{3} \approx 2.56509966$ in (24).

To check the theoretical prediction of C, we fit the dependence of $\mathrm{Re}\,\lambda \cdot \log\sigma$ with respect to $\mathrm{Re}\,\lambda$, see Fig. 3 right, by a function of the form $f(x) = A\,x + B\,x\,\log(x) - C$, $A = \log\tilde{A}$. If the fit is performed for $0.025 < \mathrm{Re}\,\lambda < 0.035$ we obtain $A \approx 6.759$, $B \approx -7.02883$ and $C \approx 2.5842$. If instead, we fit it by a function of the form $f(x) = A\,x + B\,x\,\log(x) - C + Dx^2$, we obtain $A \approx 12.9569$, $B \approx -5.25625$, $C \approx 2.5574$ and $D \approx -29.1823$, in better agreement with the predicted value of C. If we repeat the fit considering values $0.025 < \mathrm{Re}\,\lambda < 0.03$ then we obtain $A \approx 12.4998$, $B \approx -5.38492$, $C \approx 2.55925$ and $D \approx -26.9394$. Moreover, we have observed that the value of B oscillates around -6 for many of the fits performed. If we fix $B = -6$ and repeat the previous fit we obtain $A \approx 10.2986$, $C \approx 2.56783$ and $D \approx -15.9276$, in much better agreement with the expected value of C. We conjecture that the value $B = -6$ holds for the prefactor term. In any case, these fits show that the values obtained are quite robust (almost independent on the region where the fit is performed if $\mathrm{Re}\,\lambda$ is small enough) and that C approximates quite well the theoretically predicted value.

6 Dynamics near the 2D invariant manifolds $W^{u/s}(0)$

To perform direct and accurate simulations near the invariant manifolds of a hyperbolic object of a Hamiltonian system or a symplectic map is a difficult problem (see illustrations and comments in Section 6.3). Usually one aims to investigate the chaotic region which in certain cases, as

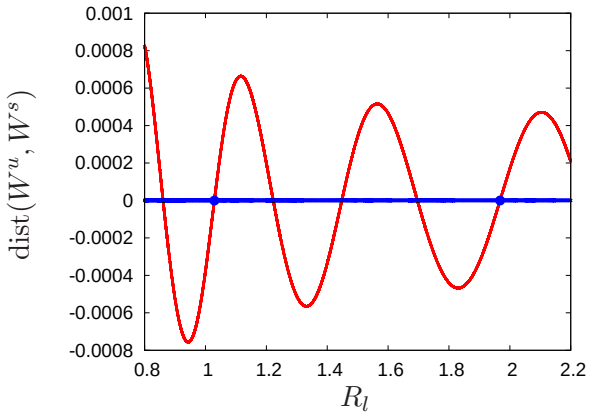

Figure 10: The graph of the unstable manifold with respect to the stable one (in the horizontal axis). R_l ranges on the x-axis. A polynomial fitting of degree 10 was performed to approximate $W^s(0)$ in the region $r_l > 0$, and used to represent the relative distance between the manifolds in the vertical axis. The two blue points correspond to consecutive iterates of the homoclinic point at $(R_l, r_l) \approx (2.730290, 0)$.

the one we are studying here, is exponentially small in the perturbation parameter ϵ. The passages close to the hyperbolic object imply then long integration times which translate in loss of accuracy. These considerations have motivated the derivation of the so-called separatrix maps which model the return to a fundamental domain near the invariant manifolds and avoid the numerical integration near the hyperbolic object.

Separatrix maps (SM) have been derived in many contexts to investigate dynamics near separatrices, we refer to [43, 6, 3, 34, 37] for details of the derivation and applications. In this section we aim to derive a return map and to suggest a first order SM model to study the dynamics of H around the 2D invariant manifolds of the CS point. The discussion below is far from being a formal derivation of the SM model but a first step in this direction. In particular, we show how to construct a fundamental domain, we study the passage time near the CS point as given by a linear approximation and we introduce suitable variables to express the SM map in a fundamental domain.

The derivation of the SM needs to be adapted to the setting here considered. In this sense, we emphasize that the reduction of the dynamics at the Hamiltonian level of the CS point to an area-preserving map was done, in previous sections, using variables that are not globally defined around the separatrices, see Fig. 8. In particular, the planar area-preserving map is only well-defined far away from the singular set $\{y_1 = 0\}$, which means that the passage near the CS point has to be described in terms of the 3-dimensional flow that defines H at the corresponding level of energy. To overtake such topological intrinsic difficulties one is lead to introduce adapted coordinates to the geometry of the problem.

The SM model we describe below will provide a model to investigate the breakdown of the invariant tori surrounding the invariant manifolds of the complex unstable point which leads to escape, see [40] for a numerical exploration of the escape in this setting.

6.1 General setting, the fundamental domain and adapted variables

Let J be the matrix of the standard symplectic form $dx\wedge dy$ in $\mathbb{R}^4$ and $z=(x,y)\in\mathbb{R}^2\times\mathbb{R}^2$. In the following, we consider an analytic Hamiltonian $H:\mathbb{R}^2\times\mathbb{R}^2\to\mathbb{R}$ such that $H(0)=\nabla H(0)=0$ and the origin is a CS equilibrium point of the Hamiltonian system $\dot z=X_H(z)=J\nabla H(z)$. We denote by $W_H^{u/s}(0)$ the corresponding 2D invariant manifolds of the origin. Furthermore, we assume that there exists a compact set $K\subset\mathbb{R}^4$ such that

a) K contains both the origin and the local invariant manifolds $W_H^{u/s}(0)$ extended up to the primary homoclinic orbits lying in their intersection,

b) the system $\dot z=X_H(z)$ is "well approximated" in K by the integrable system $\dot z=J\nabla H_n(z)$, where H_n denotes the truncation of the Sokolskii normal form $\mathrm{NF}(H)$ to order $n\geq 4$.

By "well approximated" we mean that the phase portraits of both systems are close enough, within a certain precision heuristically chosen depending on the setting and what we want to study, see related comments in Section 6.3. As an example, a Hamiltonian H above in the setting described in Section 4.1 would be a member of the family of Hamiltonians H_ν, for a given value of $\nu<0$ so that the origin is a CS point, after the transformation to Sokolskii NF up to order n, that we denoted as $\hat\phi_n$ in Section 4. That is, $H=H_\nu\circ\hat\phi_n$ for a given $n\geq 4$. Recall that at $\nu=0$ the transition to CS takes place. Also, in this setting, the compact K depends on ν as the distance up to the invariant manifolds extend also depend on the parameter and, concretely, $K=\mathcal{O}(\sqrt{\nu})$. Moreover, $H_n=\mathrm{NF}_n(H_\nu)$ (see Section 4) and hypothesis b) implies the existence of an extra first integral, that we denote by Γ_1, independent of H_n in the region of interest near the 2D separatrices of the complex-saddle fixed point, see [17]. Note that here H_n also depends on ν. Concretely, we have $H=H_n+o(\nu)$ for $n\geq 4$, see (13). Moreover, a) and b) together guarantee that $W_{H_n}(0)=W^u_{H_n}(0)=W^s_{H_n}(0)$ is a 2D pinched torus carrying on a foliation of homoclinic orbits lying on $\{H_n(z)=0,\,\Gamma_1(z)=0\}$. We recall that the system with Hamiltonian H_n is integrable while the system we are interested in, the original system H, is not. In particular, the flow associated to X_H does not preserve H_n nor Γ_1.

In the context of this work, we are interested in a planar area-preserving return map model to describe the dynamics near the separatrices within the energy level $-1-\epsilon$ of the CS point of Hamiltonian (1). However, note that to understand the return map for nearby energy levels (not containing the fixed point) is important in other problems. For example, this is the case in the analogous problem for a 4D map as mentioned in Section 2 (see also comments in Section 7).

Going back to the general setting, hereafter we consider H_n with $n\geq 4$ fixed. For the geometrical description concerning the fundamental domain below, as well as to express the associated return map, we shall use the Cartesian coordinates, given by the reduction to normal form up to order n, and the corresponding symplectic Sokolskii coordinates (R,Θ,r,θ) as introduced in (9). Recall, in particular that $\Theta=\Gamma_1$ is a formal first integral of the system. Our goal is to consider a return map to a fundamental domain `FD` within the 3D section $\hat\Sigma=\{\theta=0\}$ that captures the dynamics around the invariant manifolds. We first consider the return map to $\hat\Sigma$ defined by the integrable system H_n and after we will add the effect of the non-integrable part which is mainly reflected by the splitting of separatrices.

We construct a fundamental domain `FD` as follows. Consider a 3D neighborhood of the invariant manifolds of the integrable system of the form $|\Gamma_1|\leq\gamma_M$, for γ_M small enough, inside $\hat\Sigma$. Then:

1. Take a point $\ell\in W_{H_n}(0)\cap\hat\Sigma$ with coordinate r away from zero (for example, close to the

maximum that it takes when evaluated along $W_{H_n}(0) \cap \hat{\Sigma}$). In particular, we assume that ℓ is taken so far from $r = 0$ that the section $\hat{\Sigma}$ is transversal to $X_{H_n}(\ell)$.

2. Let $X_{H_n}^{\hat{\Sigma}}(\ell)$ be the projection of the vector $X_{H_n}(\ell)$ onto the tangent space $T_\ell(\hat{\Sigma})$. Note that since ℓ lies on a homoclinic orbit to the saddle-focus the projected vector is not the zero vector, as follows directly from equation (16).

3. Consider a local piece of a 2D surface L in $\hat{\Sigma}$ transversal to $X_H^{\hat{\Sigma}}(\ell)$.

4. Denote by $\varphi_H(t, x)$ the flow of X_H. Let L' be the first crossing of $\varphi_H(t, L)$ with $\hat{\Sigma}$ for $t > 0$. Note that the time $t = t(x)$ depends on the point $x \in L$. On the other hand, since L is chosen locally it follows that $t(x)$ is uniformly bounded from below.

5. Then $\texttt{FD}$ is the domain in $\hat{\Sigma}$ that delimit L, L' in the neighborhood $|\Gamma_1| \leq \gamma_M$ of the invariant manifolds. Note that the intersection $\texttt{FD} \cap \{H = h\}$ defines a 2D fundamental domain within the 3D energy level surface.

We introduce coordinates in $\texttt{FD}$ to derive the expression of the SM. A point $p \in \texttt{FD}$ can be identified by the energy $h = H_n(p)$ of the integrable system, the value of the first integral $\gamma = \Gamma_1(p)$ and the variable s that is defined as the evolution time of the $2\pi/\omega$-periodic Hamiltonian action φ_{Γ_1} that generates Γ_1. Recall that the action of Γ_1 preserves the H_n energy and denote by p_L the point $L \cap \{H_n = h\} \cap \{\Gamma_1 = \gamma\}$. Then $s(p) \in [0, 2\pi/\omega)$ is defined to be the unique value for which there exists $t(p)$, such that

$$\{\varphi_{H_n}(t, \varphi_{\Gamma_1}(s(p), p_L)), 0 \leq t \leq t(p)\} \subset \hat{\Sigma} \qquad \text{and} \qquad \varphi_{H_n}(t(p), \varphi_{\Gamma_1}(s(p), p_L)) = p, \tag{25}$$

where φ_{H_n} refers to the action (the flow) associated to the integrable Hamiltonian H_n. Each of the flows φ_{H_n} and φ_{Γ_1} defines a foliation in $\hat{\Sigma} \cap \texttt{FD}$. Moreover, $\{H_n, \Gamma_1\} = 0$ and these foliations are independent, see Fig. 11 for a sketch. We also refer to [33] where a complete description of the integrable dynamics is obtained in terms of both first integrals in involution and their corresponding evolution times.

The transformation $\mathcal{T} : (x_1, x_2, y_1, 0) \mapsto (h, \gamma, s)$ is well-defined for $|h| < h_M$ small (here $h = H_n(x_1, x_2, y_1, 0)$, $\gamma = \Gamma_1(x_1, x_2, y_1, 0)$ and s is given as explained above) and defines a change of coordinates in $\texttt{FD}$. Note that a single iteration of SM shiftes s by $t \,(\mathrm{mod}\, 2\pi)$, where t is the time required to return to $\texttt{FD}$. The corresponding return map SM preserves a suitable area-form $g(\gamma, s) d\gamma \wedge ds$.

6.2 The inner and gluing maps

As usual, see [34], the separatrix return map SM: $\texttt{FD} \to \texttt{FD}$ is obtained as the composition of two maps: the *inner map* modeling the passage near the hyperbolic object and the *gluing map* modeling the reinjection to the fundamental domain. In our setting, the SM will be a one-parameter family of 2D separatrix maps $\mathrm{SM}_{\hat{h}}$ expressed in coordinates (γ, s) and parameterized by the preserved energy level $\hat{h}$ of the non-integrable Hamiltonian H.

The inner map. The inner map concerns the passage near the CS fixed point. The normal form around a hyperbolic CS fixed point was studied in [11], in the $\mathcal{C}^\infty$ case, and in [35], in the analytic one. Here we simply reformulate the result following [27], see also [33], and we refer to the original references for the proofs. Consider a CS fixed point with eigenvalues $\pm\alpha \pm i\omega$, $\alpha, \omega > 0$. The statement adapted to our setting reads as follows.

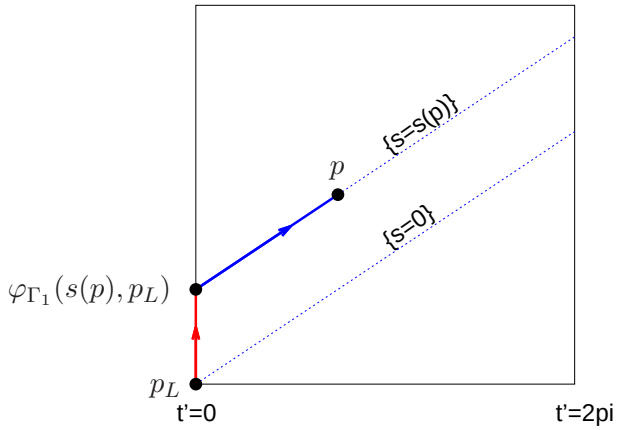

Figure 11: Schematic representation of the independent actions of Γ_1 and H_n on the torus where the coordinates $(t', s) \in [0, 2\pi) \times [0, 2\pi/\omega)$ are defined. Here t' is a normalization of the time t so that $t' \in [0, 2\pi)$. Such a torus lies inside $\{H = h\} \cap \{\Gamma_1 = \gamma\}$ for given h and γ. By uniqueness of solutions of the corresponding Cauchy problems, such actions define the coordinate $s(p)$ through relation (25), see text. The action of Γ_1 is represented vertically (in red). The action of H_n is represented as an inclined line (in blue). The labels p, p_L and $\varphi_{\Gamma_1}(s(p), p_L)$ indicate the projection onto the coordinates (t', s) of those points.

Theorem 6.1. *Let H_n be the truncation of the Sokolskii normal form to order $n \geq 4$. Then, there exist a neighborhood $\mathcal{U}$ of the CS point and symplectic coordinates (x_1, x_2, y_1, y_2) defined in $\mathcal{U}$ such that*

$$H_n = -\omega\Gamma_1 + \alpha\Gamma_4 + F_n(\Gamma_1, \Gamma_4),$$

where $\Gamma_1 = x_2y_1 - x_1y_2$, $\Gamma_4 = x_1y_1 + x_2y_2$ and F_n is a real analytic function of order 2.

We are interested in a small neighborhood of the invariant manifolds of the CS point, hence we simply use the linear vector field associated to the quadratic Hamiltonian function provided by the previous result, that we denote by $H_2 = -\omega\Gamma_1 + \alpha\Gamma_4$, to obtain an approximation of the inner map. The linear passage near a CS point was studied in [9]. The stable invariant manifold is given by $x_1 = x_2 = 0$ while $y_1 = y_2 = 0$ corresponds to the unstable one. In polar coordinates $x_1 = r_u \cos\theta_u$, $x_2 = r_u \sin\theta_u$, $y_1 = r_s \cos\theta_s$ and $y_2 = r_s \sin\theta_s$ the linear equations are $\dot{r}_u = \alpha\, r_u$, $\dot{\theta}_u = \omega$, $\dot{r}_s = -\alpha\, r_s$ and $\dot{\theta}_s = \omega$. Hence, the flight time from the 3D section $\Pi_0 = \{r_s = 1\}$ to $\Pi_1 = \{r_u = 1\}$ is $t_v = -\log(r_u^0)/\alpha$, where r_u^0 refers to the r_u-coordinate of the initial point on Π_0. Accordingly, the s variable evolves as $s \mapsto s + t_v \pmod{2\pi}$ during the inner passage.

Finally, we need to express the flight time t_v as a function of the coordinates h, γ. Here h refers to an energy level of H_2, which is close to the energy level of H_n in a small neighborhood of the CS point. The relations $r_s^0 = 1$, $\gamma = r_u^0 \sin(\theta_u - \theta_s)$ and $\omega\gamma + h = \alpha r_u^0 \cos(\theta_u - \theta_s)$ lead to

$$(\alpha\gamma)^2 + (\omega\gamma + h)^2 = (r_0^u)^2\alpha^2,$$

that gives the following expression for the flight time

$$t_v = t_v(h, \gamma) = -\frac{1}{\alpha} \log\left(\frac{1}{\alpha}\sqrt{(\alpha\gamma)^2 + (\omega\gamma + h)^2}\right). \tag{26}$$

We observe that

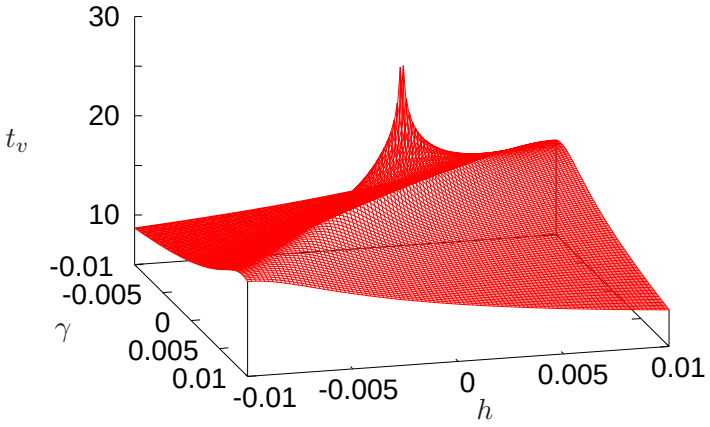

Figure 12: For $\omega = 1$, $\alpha = \sqrt{0.1}$ we represent the flight time $t_v(\gamma, h)$ as given by (26).

- If $\omega\gamma + h = 0$ then
$$t_v(h,\gamma) = t_v(\gamma) = -\frac{1}{\alpha}\log|\gamma| + \mathcal{O}(\alpha).$$
- If $\omega\gamma + h \neq 0$ then
$$t_v(h,\gamma) = -\frac{1}{\alpha}\log\left|\frac{\omega\gamma + h}{\alpha}\right| + \mathcal{O}(\alpha).$$

In Fig. 12 we represent $t_v(h,\gamma)$ for $\omega = 1$, $\alpha = \sqrt{0.1}$. Compare with Fig. 20 in Appendix D where we numerically compute the return time to two different Poincaré sections for the integrable system given by Hamiltonian $\mathrm{NF}_4(H)$.

Introducing $\hat{b} = -1/\alpha < 0$ we can express the flight time (26) as $t_v(h,\gamma) = (\hat{b}/2)\log(\gamma^2 + \hat{b}^2(\omega\gamma + h)^2)$. We emphasize that in the setting of Section 4.1 one has $\hat{b} = \mathcal{O}(1/\sqrt{-\nu})$.

The gluing map. The local coordinates used for the inner map can be extended by forward/backward integration so that define two coordinate sets on the FD. The gluing map identifies both coordinate sets by taking into account the effect of the relative position of the split separatrices. This is given by the splitting function $\mathcal{M}(s)$.

In a perturbative regime one can derive a more concrete expression for $\mathcal{M}(s)$. To this end, we recall that for generic analytic area-preserving maps, like the return map to $\mathtt{FD} \cap \{H = h\}$ we aim to construct, the first harmonic of the splitting function is expected to become the dominant one when the perturbation from the integrable limit is small enough, see [3, 7]. Other more complicated contexts, like the one for a 4D map mentioned in Section 2, might lead to a quasi-periodic representation of the spliting function.

The setting of Section 4.1 falls into the previous perturbative case. Therefore, according to the considerations in Section 5.1, the splitting function is expected to behave asymptotically as $A(\nu)\sin(2s)$ when $\nu \to 0$, where the factor 2 can be inferred from the computations displayed in Fig. 10. Note that a shift along the s variable and a normalization of s is needed to get the previous expression for the splitting function. We will assume that s changes to $s + \hat{a} + t_v$ for some

constant $\hat{a} \in [0, 2\pi)$. The constant $A(\nu)$ accounts for the splitting amplitude. In Section 5.2 we checked that the asymptotic behavior of the splitting angle is exponentially small in $\delta = \sqrt{-\nu}$ and, consequently, so it is the asymptotic behavior of the amplitude $A(\nu)$.

The suggested separatrix map model. Previous considerations suggest that, at first order, a suitable model of the integrable three-dimensional return map to $\mathtt{FD} \subset \mathbb{R}^2 \times \mathbb{R}/2\pi\mathbb{Z}$ is given by

$$\begin{pmatrix} h \\ \gamma \\ s \end{pmatrix} \longmapsto \begin{pmatrix} h' \\ \gamma' \\ s' \end{pmatrix} = \begin{pmatrix} h \\ \gamma \\ s + \hat{a} + \frac{\hat{b}}{2} \log\left(\gamma^2 + \hat{b}^2(\omega\gamma + h)^2\right) \end{pmatrix}, \tag{27}$$

where h and γ refer to the values of the first integrals of the integrable system H_n, with $n \geq 4$, and Γ_1, respectively.

Next we add the effect of the separatrix splitting to the previous integrable return map. As already mentioned, when considering the system defined by the Hamiltonian H the quantities H_n and Γ_1 are no longer preserved. The intersections of the 3D section $\hat{\Sigma} = \{\theta = 0\}$ with the level sets of H_n and H are two close families of 2D manifolds. The Poincaré maps associated to H_n and H are also close (because hypothesis b in Section 6.1). We assume that the transformation $(h, \gamma, s) \mapsto (H(h, \gamma, s), \gamma, s)$ defines a change of variables on $\hat{\Sigma}$ (at least, locally around $W^{u/s}(0)$). Denoting by $\hat{h} = H(h, \gamma, s)$ the inverse transformation is given by $(\hat{h}, \gamma, s) \mapsto (H_n(\hat{h}, \gamma, s), \gamma, s)$.

We consider $\hat{h}$ to be the level set of H containing the CS fixed point. Since $\hat{h}$ remains constant (because H is a first integral), inside $\{H = \hat{h}\}$ we can then consider the energy H_n as a function of the variables γ and s, that is, we write $h = H_n(\gamma, s)$. Then, by substituting it into the expression (27) we obtain a separatrix return map $\mathtt{FD} \cap \{H = \hat{h}\} \to \mathtt{FD} \cap \{H = \hat{h}\} \subset \mathbb{R} \times \mathbb{R}/2\pi\mathbb{Z}$ of the form

$$\begin{pmatrix} \gamma \\ s \end{pmatrix} \longmapsto \begin{pmatrix} \gamma' \\ s' \end{pmatrix} = \begin{pmatrix} \gamma + A(\nu)\sin(2s) \\ s + \hat{a} + \frac{\hat{b}}{2} \log\left(\gamma^2 + \hat{b}^2\left(\omega\gamma + H_n(\gamma, s)\right)^2\right) \end{pmatrix}, \tag{28}$$

where we have added the effect of the perturbation as a displacement of γ according to the considerations in the discussion of the gluing map.

In the following we shall assume that $|H_n(\gamma, s)|$ is small enough so that can be ignored in the approximation of the dynamics given by (28). Note that we ignore the correction produced by the term $|H_n(\gamma, s)|$ in a very small neighborhood of the invariant manifolds since the range of interest of the variable γ in (28) is exponentially small in ν. As $H = H_n + o(\nu)$, taking ν small enough such assumption holds true. The previous considerations let us to consider the return map

$$\begin{pmatrix} \gamma \\ s \end{pmatrix} \longmapsto \begin{pmatrix} \gamma' \\ s' \end{pmatrix} = \begin{pmatrix} \gamma + A(\nu)\sin(2s) \\ s + \tilde{a} + \hat{b}\log|\gamma'| \end{pmatrix}, \tag{29}$$

where $\tilde{a}, \hat{b} \in \mathbb{R}$. We note that

- $\tilde{a} = a + \hat{b}\log(\omega) + \hat{b}\log|\hat{b}|$, (mod 2π),
- we have ignored terms of relative size $\mathcal{O}(b^{-2})$ in the second component, and
- we have substituted γ by γ' in order to obtain an area-preserving return map.

Since we want to study the dynamics around the invariant manifolds $W^{u/s}(0)$ and, concretely, in a neighborhood of the order of the size of the splitting, we introduce scaling variables $s \mapsto s/2\pi$,

$\gamma \mapsto \gamma/A(\nu)$, so that the previous map (29) becomes

$$\begin{pmatrix} \gamma \\ s \end{pmatrix} \longmapsto \begin{pmatrix} \gamma' \\ s' \end{pmatrix} = \begin{pmatrix} \gamma + \sin(4\pi s) \\ s + a + b\log(|\gamma'|) \end{pmatrix},$$

where $a = \tilde{a}/2\pi + b\log(2\pi|A(\nu)|) + b\log|b| \pmod 1$ and $b = \hat{b}/2\pi$.

Note that the obtained return map (28) only differs from the usual (first order) separatrix map, see e.g. [37], in the dependence of the constant a with respect to the parameter b. This is because the expression of the flight time obtained near the CS hyperbolic fixed point which differs from the flight time near a saddle fixed point of a 1-DOF Hamiltonian. This modification does not play any relevant role in the main properties of the chaotic zone (but may affect details of the dynamics inside the chaotic zone, see [38] for a discussion on the dependence of the parameters a and b and the relation with the abundance of islands within homoclinic lobes in one parameter families of maps). In particular, the approximation of the separatrix map by a Chirikov standard map at some distance from the separatrices provides the following description of the chaotic zone, see [37] for details:

- The distance d_c from the separatrices to the closest invariant curve bounding the chaotic region is $\gamma \sim d_c \approx 2|b|/k_G$, where $k_G \approx 0.97...$ is the so-called Greene constant.
- Approximately $1.415\,b$ chains of (rotational) islands are expected to be found within the chaotic zone created by the splitting of the separatrices, and these islands are expect to appear from distance $\gamma \sim d_i \approx 2|b|/\pi$ on, measured from the separatrices.

6.3 On the difficulties to describe the chaotic zone near $W^{u/s}(0)$

The SM map model above derived aims to describe the dynamics in a tubular region near the invariant manifolds $W^{u/s}(0)$. In the derivation, one assumes the relevant parameter to be close enough to the bifurcation parameter where a Hamiltonian-Hopf takes place. Moreover a first order approximation of the flight-time and of the splitting function restrict the parameters for which SM provides useful approximation. Hence, even though the SM model derived might be useful to describe the dynamics within the chaotic zone where direct numerics simulations are not feasible, to find a suitable range of parameters where to compare the approximation of the SM with the actual dynamics is a difficult problem. We refer to [37] for further comments in this direction and for comparisons and illustrations in a simpler framework.

In order to illustrate the difficulties, we consider the original Hamiltonian (1) with the usual parameters (6) and $\epsilon = -0.5$ (hence $\nu = -0.0\overline{5}$), as in Fig. 8. Note that one cannot consider $|\nu|$ too small since then the splitting and the chaotic region cannot be detected within the precision used in simulations (here we restrict ourselves to double precision simulations). We compute numerically the return map by a direct integration of the original Hamiltonian (1). In Fig. 13 we show details of the phase space of the return map to $\Sigma = \{\theta_l = 0\}$ restricted to the level of energy of the CS point (that is, the linear coordinates are used). One can see that the chaotic region extends for $2.712 \lessapprox r_l \lessapprox 2.7796$, where we can observe invariant curves bounding the bounded chaotic component near the invariant manifolds. A preliminary numerical exploration of the chaotic zone size performing numerical integrations of initial conditions in the chaotic zone and iterating them up to $t = 10^7$ indicates that the width of the chaotic region seems to be $\approx 7 \times 10^{-2}$. For $r \approx 2.7796$ there seems to be an invariant curve but it is difficult to assert it properly due to cantori surrounding the different chains of islands that form an effective barrier

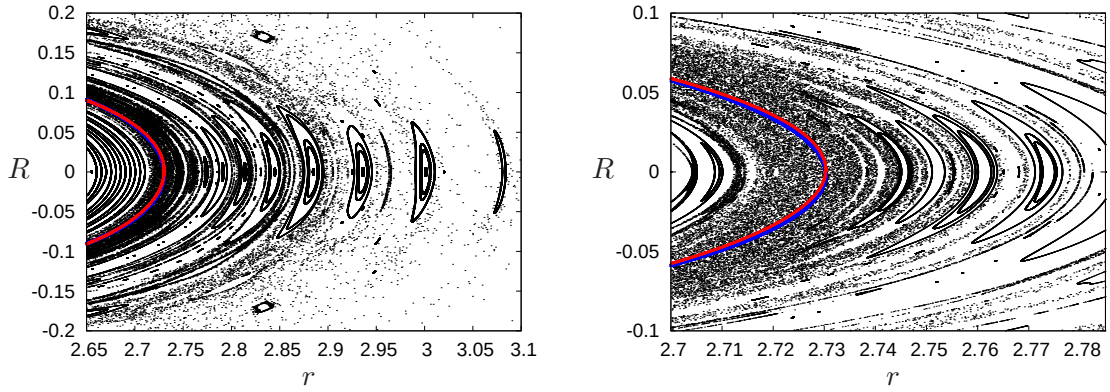

Figure 13: Phase space of the Poincaré return map to $\Sigma = \{\theta = 0\}$ for $H = -1 - \epsilon$, $\epsilon = -0.5$ (energy level of the CS point). We also display $W^{u/s}(0)$. Left: Different chains of islands, even in the open chaotic region, are observed. Right: We can see further details of the bounded chaotic zone created by the splitting of the invariant manifolds.

to global diffusion (it might be also possible that, for $\epsilon = -0.5$, orbits outside the invariant manifolds escape after a big enough number of iterations). On the other hand, several chains of islands are detected and they extend to the open chaotic region for $r_l \gtrapprox 2.82$.

Fig. 14 shows the predicted position of the invariant manifolds for the approximations obtained by $\mathrm{NF}_4(H)$ and $\mathrm{NF}_8(H)$ respectively. See Sections 4.1 and 5 for details on the applied changes of variables.

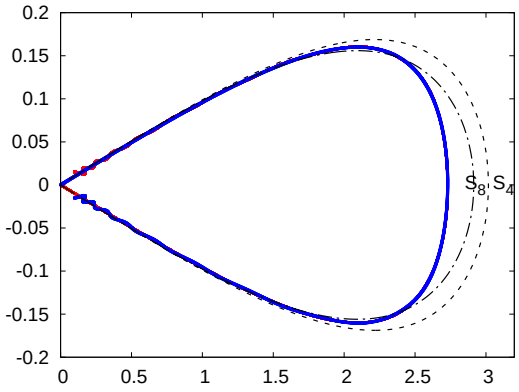

Figure 14: In blue/red we display $W^{u/s}(0)$ for the Poincaré return map to $\{\theta = 0\}$ with $H = -1 - \epsilon$ (energy level of the CS point). The black discontinuous curves represent the intersection of the 3D set $\Gamma_1 = 0$ with the section $\{\theta = 0\}$, where Γ_1 is computed for $\mathrm{NF}_k(H)$ with $k = 4$ and $k = 8$ respectively.

We note that:

- Increasing the NF truncation order we can obtain a better approximation of the true position of $W^{u/s}(0)$. This is expected up to an optimal truncation order, see Remark 4.2. In the example, the obtained approximations are far from giving an accurate description. We have also checked that using $\mathrm{NF}_{12}(H)$ we obtain a slightly better approximation but still far from being accurate.

- The return map model will predict invariant curves bounding the chaotic zone created by the breakdown of the invariant curves and that these are expected to be located at the same distance, inside and outside, from the predicted location of the invariant manifolds.
- Maybe $\epsilon = -0.5$ gives $|\nu|$ too large to obtain a satisfactory description of the dynamics in Fig. 13 by a return limit map as the SM map. But smaller values of $|\nu|$ will require longer computations because the flight time close to the CS point becomes larger, and will require high order precision arithmetics since the width of the chaotic zone decreases exponentially in $|\nu|$.

We believe that the SM model proposed in this work provides a first order approximation to investigate dynamics for small values of $|\nu|$ where direct numerics becomes difficult. However, further comparisons and a more rigorous analytical derivation is necessary to understand the range of values and the limitations of the model.

7 Conclusions and future work

In this paper we have explored the dynamics of a family of 2-DOF Hamiltonian systems after a complex-saddle transition of an equilibrium point. The considered family is close to a family of integrable Hamiltonians (given by the truncated Sokolskii NF) which has bounded manifolds.

We have computed the 2D invariant manifolds of the equilibrium point and we have used two different Poincaré sections to visualize the phase space geometry in a region containing the invariant manifolds.

Furthermore, we have computed the homoclinic trajectories and the splitting angle between these invariant manifolds. In particular, we have obtained precise exponentially small estimates (in a parameter which measures the distance to the bifurcation) of their splitting angle. We have obtained a formula, very close to the analytical upper bounds, that depends on a complex singularity of the homoclinic trajectory of an auxiliary integrable system (as it happens in related problems). We have numerically checked, using multiprecision arithmetics, that this formula accurately describes the asymptotic behavior of the angle.

The spliting of the invariant manifolds creates a chaotic zone near them. The exponential small size of this zone makes it difficult to detect numerically by iteration of the Poincaré map. To investigate the dynamics in this chaotic zone near the 2D invariant manifolds we have detailed the steps involved in a derivation of a separatrix return map. The obtained return map models the dynamics in the mentioned zone. The return map description of the dynamics becomes more accurate as the parameter becomes smaller, that is, in the regime where direct simulations are out of reach.

Certainly, some of the results of this work require a more detailed analytical explanation. We hope that the explorations here can help in this direction. As examples we mention the following two points:

- The discussion of the behavior of the splitting of the 2D invariant manifolds $W^{u/s}(0)$ is based on estimates of the upper bounds. It would be interesting to provide sharp upper and lower bounds to fully describe the asymptotic behavior of such splitting.
- The derivation steps leading to the SM model in this setting need to be rigorously justified.

It would also be interesting to estimate the error of the SM model to quantitatively describe the dynamics in a neighborhood of the invariant manifolds.

To conclude with, we recall that, as pointed out in the Introduction and in Section 2, the system (1) considered through the paper appears as a local model near double resonances of a 4D symplectic map. The phase space geometry of this model is relevant for the Arnold diffusion problem in the so-called non-definite setting, where diffusion is expected to be much slower and there are few available results. We remark that:

- The 2D invariant manifolds of the CS point allow points to cross the junction of the resonances and locally accelerate the diffusion process along the single resonance. The geometry of the invariant manifolds is similar to the geometry of the ones of the 2-DOF Hamiltonian system shown here.
- Generically, the preservation of the two formal integrals that provide the Sokolskii NF will no longer hold. The splitting of the invariant manifolds is expected to be exponentially small in ν but a quasi-periodic effect might emerge in such splitting behavior due to the interaction of the internal frequency with the external one related to the discretization. We refer to [17] for a description of the behavior of the splitting of the invariant manifolds of a CS equilibrium point of a (2+1/2)-DOF Hamiltonian system.
- A derivation of a suitable return map adapted to this setting would allow to explore the chaotic dynamics near the invariant manifolds generated by such splitting. Note that the methodology described in this paper for the derivation of the return map would be also applicable in this context.

We aim to consider the analogous explorations to those presented here in the setting of 4D symplectic maps elsewhere.

Acknowledgments

This work has been supported by grants PID2019-104851GB-I00 (Spain) and 2017-SGR-1374 (Catalonia). We also acknowledge the Severo Ochoa and María de Maeztu Program for Centers and Units of Excellence in R&D (CEX2020-001084-M). We are indebted to C. Simó for his guidance and suggestions, as well as for many of the ideas reflected in this work. We also thank J. Timoneda for the technical support on the computing facilities of the Dynamical Systems Group of the Universitat de Barcelona that have been largely used in this work.

A Numerical solution of the homological equation via the Fredholm alternative

As explained in Section 4.1 to normalize the order (k, j) terms we look for a polynomial Hamiltonian $G \in \mathbb{P}_k$ such that

$$H_{k,j} + \mathrm{ad}_{H_2}(G) \in \mathrm{Ker}\,\mathrm{ad}_{H_2}^{\top}.$$

Hence we have to obtain numerically the following factorization

$$\mathbb{P}_k = \mathrm{Im}\,\mathrm{ad}_{H_2} \oplus \mathrm{Ker}\,\mathrm{ad}_{H_2}^{\top},$$

at each order k. This can be easily obtained in the following way:

1. We consider the canonical basis $e_1, \dots, e_N$ of $\mathbb{P}_k$ given by the monomials $x_1^i x_2^j y_1^s y_2^t$ ordered according to the reverse lexicographical order. Note that $N = \dim \mathbb{P}_k = (k+3)!/(6(k!))$. Let $A \in \mathbb{R}^{N\times N}$ be the matrix representation of the linear operator ad_{H_2} in this basis.

2. We express the generating Hamiltonian G in terms of the canonical basis, i.e. $G = a_1 e_1 + \cdots + a_N e_N$. Our unknowns are then $\mathbf{a} = (a_1, \dots, a_N)$. Similarly, let $\mathbf{h} = (h_1, \dots, h_N)$ be the representation of $H_{k,j}$ in terms of the canonical basis. The idea is to solve the homological equation
$$A\,\mathbf{a} = -\mathbf{h}.$$
Since $\operatorname{Ker} A \neq \emptyset$ the previous equation does not have a unique solution.

3. The Fredholm alternative give us a systematic way to choose a solution of the homological equation for all orders k. First we determine a basis of $\operatorname{Im} A$. To this end we apply a Gaussian elimination procedure with column pivoting to $A^\top$. The non-zero rows after the process generate $\operatorname{Im} A$ hence we remove from A the corresponding columns. Assume that $M = \dim(\operatorname{Im} A)$. Denote by $\tilde{A} \in \mathbb{R}^{N\times M}$ the reduced matrix after removing the columns and by $\tilde{\mathbf{a}} \in \mathbb{R}^M$ and $\tilde{\mathbf{h}} \in \mathbb{R}^M$ the vectors obtained from $\mathbf{a}$ and $\mathbf{h}$ respectively by removing the corresponding components.

4. The Sokolskii NF reduction (10) shows that $\operatorname{Ker} A^\top$ is generated by $\mathcal{I}(\Gamma_1, \Gamma_3) \cap \mathbb{P}_k$, where $\mathcal{I}(\Gamma_1, \Gamma_3)$ stands for the ideal of the ring of polynomials in four variables generated by Γ_1 and Γ_3. In particular, $N - M = \dim(\mathcal{I}(\Gamma_1, \Gamma_3) \cap \mathbb{P}_k) = N - \dim(\operatorname{Ker} A)$.

5. Denote by $g_1, \dots, g_{N-M}$ the elements of $\mathcal{I}(\Gamma_1, \Gamma_3) \cap \mathbb{P}_k$. They form a basis of $\operatorname{Ker} A^\top$. Express g_i in terms of the canonical basis of $\mathbb{P}_k$. Define $B \in \mathbb{R}^{N\times N}$ by completing $\tilde{A}$ adding the columns $g_1, \dots, g_{N-M}$. We also add to the unknowns $\tilde{\mathbf{a}}$ a set of unknowns $\alpha_1, \dots, \alpha_{N-M}$ and we complete the vector $\tilde{\mathbf{h}}$ adding 0's in the remaining components. Denote by $\hat{\mathbf{a}}$ and $\hat{\mathbf{h}}$ the obtained vectors.

6. Finally we solve the (consistently determined) linear system of equations
$$B\,\hat{\mathbf{a}} = -\hat{\mathbf{h}}.$$
In this way we obtain the coefficients $\mathbf{a}$ (one has to complete $\tilde{\mathbf{a}}$ by adding zeros in the removed components). The coefficients $\alpha_1, \dots, \alpha_{N-M}$ are the coefficients of the linear combination of the terms $\hat{H}_{k,j}$ of the normalized Hamiltonian in terms of the basis $g_1, \dots, g_{N-M}$ of $\operatorname{Ker} A^\top$.

The above procedure allows to compute the generating Hamiltonian G. Then, selecting a proper strategy to eliminate order by order the terms, we can formally (i.e. ignoring the storage limitations due to the memory capabilities of the computer) compute the changes of coordinates to obtain the Sokolskii NF for the Hamiltonian-Hopf bifurcation up to any desired order.

B On the set of parameters a_2, a_3 for which the NF Hamiltonian has non-bounded manifolds after the CS transition

In this appendix we consider the Hamiltonian (1) and we explore the boundedness of the manifolds $W^{u/s}(0)$ for different values of the parameters a_2 and a_3. These parameters have to verify

$a_3 - a_2^2 < 0$ since otherwise the origin of the Hamiltonian system (1) does not undergo a CS transition. It is enough to consider $a_2 > 0$ (otherwise consider $J_1 \mapsto -J_1$, $\psi_1 \mapsto -\psi_1$). Recall from (13)-(14) that, for NF(H_δ), the invariant manifolds are bounded provided $\eta > 0$. For $\eta < 0$ the invariant manifolds are not locally bounded. According to (11)–(13), the higher order terms of the Hamiltonian on the manifolds are of the form $\delta^{k_1}\Gamma_3^{k_2}$ for some $k_1, k_2 \in \mathbb{N}$, $k_1 \geq 2$, $k_2 \geq 1$, being $\delta^2\Gamma_3^3, \delta^3\Gamma_3$ the dominant ones. But since $2\Gamma_3 = y_1^2 + y_2^2$, these terms do not force the invariant manifolds to be bounded (in the domain where the optimally truncated NF gives a good approximation, see Remark 4.2).

In Fig. 15 we represent in blue the region of parameters for which η is negative. To get such a figure we have numerically computed the reduction to the form (11) for values of a_2, a_3 in a mesh of points, exactly as we did in Section 5 for the values $a_2 = 1/2$ and $a_3 = -3/4$. The figure shows that the condition to have $\eta < 0$ is $2|a_2| - 1 < a_3 < a_2^2$. The corresponding lines bounding the blue region are represented in red in the figure.

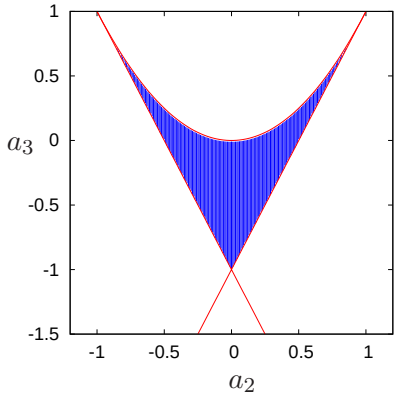

Figure 15: Region of (a_2, a_3)-parameters for which $\eta < 0$, hence with non-bounded invariant manifolds $W^{u/s}(0)$ (for the NF). Also the lines bounding the previous region are shown in red.

C Comments on "the passage by the maximum" section

In appropiate coordinates, the original system (1) can be considered as a small perturbation of the system (13), ignoring the $\mathcal{O}(\delta^2)$-terms, that is, it becomes close to the system $\dot{z} = X_0(z) = J\nabla H_0(z)$ where $z = (x_1, x_2, y_1, y_2)$ and

$$H_0 = -\Gamma_1 + \delta\left(\Gamma_2 + a\Gamma_3 + \eta\Gamma_3^2\right). \tag{30}$$

Note that, comparing with (13), with the aim of lighten the notation, we have omitted the $\sim$ on the scaled variables.

We consider the section Π taken at the passage by a maximum of $\Gamma_3 = (y_1^2 + y_2^2)/2$. Note that for any truncation of the normal form system (10), and also for the rescaled system (30), one has $\frac{d}{dt}\Gamma_3 = 0$ if, and only if, $\Gamma_4 = 0$, where $\Gamma_4 = y_1x_1 + y_2x_2$. Note that this condition is equivalent to $R = 0$ if $r > 0$, see (9) and Fig. 5.

Remark C.1. The section Π at the passage by the maximum of Γ_3 was used in [17] for exploring the splitting of the invariant manifolds of the CS of a periodic forcing of an integrable system for which the CS has a 2D homoclinic manifold. This is the main reason why we consider it here.

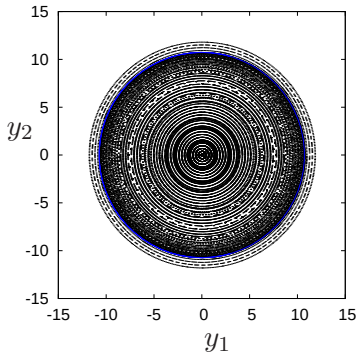

Figure 16: We display return map iterates obtained from the integrable system (30) with $a = -9/32$, $\eta = 5/1024$ and $\delta = \sqrt{\epsilon - \epsilon_c}$ with $\epsilon = -0.5$. The invariant manifolds form a circle of radius ≈ 10.73 in the coordinates (y_1, y_2) shown.

Let us discuss about the transversality properties of the section Π. Consider first the system (30). For this system one has $\langle X_0, \nabla\Gamma_4\rangle = 0$ for

$$\Gamma_2 = \Gamma_3(a + 2\eta\Gamma_3). \tag{31}$$

This relation defines a 3-dimensional manifold where the section Π is non-transversal. On the other hand, system (30) possesses Γ_1 as an additional first integral. We claim that this implies that $\{\Gamma_1 = 0\} \cap \Pi = \{\Gamma_2 = 0\} \cap \Pi$. To see this, note that one has $W_H^{u/s}(0) \subset \{H = \Gamma_1 = 0\}$. Then $\Gamma_2 + a\Gamma_3 + \eta\Gamma_3^2 = 0$ on $W_H^{u/s}(0)$. It follows that $W_H^{u/s}(0) \cap \{\Gamma_2 = 0\} \neq \emptyset$ if, and only if, $\Gamma_3 = 0$ or $\Gamma_3 = -a/\eta$. On the other hand, the orbital derivative of the function $\Gamma_3(z)$ along solutions of $\dot{z} = X_H(z)$ is

$$\frac{d}{dt}\Gamma_3 = -\delta\Gamma_4.$$

If $x = (x_1, x_2)$ and $y = (y_1, y_2)$, then the condition of being extrema implies $\langle x, y\rangle = 0$. But, the condition $\Gamma_1 = 0$ means that $\langle x, y^\perp\rangle = 0$, meaning that extrema of Γ_3 on $W^{u/s}(0)$ is reached whenever $x = 0$, that is, for points on $\{\Gamma_2 = 0\}$.

Hence, the non-transversality relation (31) reduces to $\Gamma_3(a + 2\eta\Gamma_3) = 0$. Then we obtain that, apart from the origin, transversality is lost on the circumference $y_1^2 + y_2^2 = -a/\eta$, $x_1 = x_2 = 0$ (recall that $a < 0$ and $\eta > 0$ in the bounded case). Moreover, the second order orbital derivative of Γ_3, is

$$\frac{d^2}{dt^2}\Gamma_3 = -2\delta^2\left(\Gamma_3(a + 2\eta\Gamma_3) - \Gamma_2\right), \tag{32}$$

that, when evaluated at $\Gamma_2 = 0$ and $\Gamma_3 = -a/\eta$, is negative. We conclude that the intersection $W_H^{u/s}(0) \cap \{\Gamma_2 = 0\} \cap \Pi$ is the circumference $y_1^2 + y_2^2 = -2a/\eta$, $x_1 = x_2 = 0$. This implies transversality of the section Π in a neighborhood of the invariant manifolds $W^{u/s}(0)$. Fig. 16 shows iterates of the return map to Π for the integrable system (30) with $a = -9/32$, $\eta = 5/1024$ and $\delta \approx 0.2357$ which corresponds to $\epsilon = -0.5$.

We emphasize however that our goal is to use the section Π to investigate the original system (1). For such a system, Γ_1 is not a first integral but simply a formal first integral. This has important consequences concerning the transversality properties of Π. To describe the loci of points where transversality fails we proceed as follows. Let $x = (x_1, x_2)$, $y = (y_1, y_2)$, then $2\Gamma_2 = x^\top x = X^2$, $2\Gamma_3 = y^\top y = Y^2$ where $X = \pm\|x\|_2$ and $Y = \pm\|y\|_2$. The condition (31) reads $X^2 - aY^2 + \eta Y^4 = 0$. The signs of X and Y determine two curves where the section Π is not

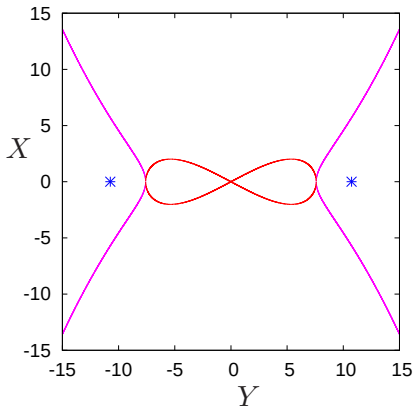

Figure 17: For parameters (6), we show the curves in Y, X-variables where the section Π is non-transversal. Each of these curves corresponds to a 2D surface within the 3D energy level of the CS point. The two points correspond to the 1D intersection with Π of the 2D invariant manifolds of the CS point for the limit system obtained by the truncation to order four of the Sokolskii NF for $\nu \to 0$. In the (y_1, y_2) coordinates these points correspond to a circle. See text for details. The figure shows that there are points of non-transversality of Π in any tubular region of the invariant manifolds for any perturbed (non-integrable) nearby system.

transversal. For positive signs the curve is bounded away from the invariant manifolds $W^{u/s}(0)$. For alternate signs however the curve extends to infinity. The whole picture is shown in Fig. 17 for parameters (6). We summarize the geometrical meaning of this plot in the following items:

- Each of the curves shown in the Y, X-plane corresponds to a 3D surface embedded in the 4D space (in x, y coordinates). Restricted to the zero energy level of the complex-saddle point of the original Hamiltonian (in Cartesian coordinates) they are 2D manifolds and, hence, they define a 1D intersection manifold with Π. We denote this 1D intersection by $\mathtt{NT}_1$, recall that it corresponds to points where the section is non-transversal.
- On the other hand, for $|\nu|$ small, the 2D $W^{u/s}(0)$ lie inside the 3D surface of constant energy equals zero and intersect Π near the 1D curve $W_1 : \{y_1^2 + y_2^2 = -2a/\eta\}$, since the system is a perturbation of such a case. In the Y, X-coordinates this curve is seen as two points on the $X = 0$ axis.
- The curves $\mathtt{NT}_1$ and W_1 intersect at four points in Π. This follows from the fact that, along the curves of $\mathtt{NT}_1$ corresponding to alternate signs of X and Y, the Y variables ranges from values less than $\sqrt{-2a/\eta}$ to larger values.

The curves $\mathtt{NT}_1$ where Π become non-transversal are present in all the illustrations below and they reflect the intriguing topology of the Hamiltonian-Hopf singularity.

One might expect another section to be transversal in a neighborhood of the invariant manifolds $W^{u/s}(0)$ of the non-integrable system. However, the previous considerations imply that any candidate section that is invariant by the formal symmetry of the Sokolskii NF becomes singular for points on $W^{u/s}(0)$ of a non-integrable system. Let us state this fact rigorously.

Proposition C.1. *Let H be any non-integrable Hamiltonian perturbation of (30), both having the same jet up to order 4. Denote by X the corresponding vector field. Let $W^{u/s}(0)$ be the*

invariant manifolds of the CS point of X, $\delta > 0$. Let $\Pi \subset \mathbb{R}^4$ a three-dimensional C^1-manifold invariant by the action of the rotation group generated by Γ_1. Then, there is $z \in \Pi \cap W^{u/s}(0)$ such that $X(z) \in T_z\Pi$.

Proof. By hypothesis $X = X_0 + \mathcal{O}(\delta^2)$ being $X_0 = (-x_2 + \delta y_1(a + \eta(y_1^2 + y_2^2)), x_1 + \delta y_2(a + \eta(y_1^2 + y_2^2)), -y_2 - \delta x_1, y_1 - \delta x_2)$. Assume that $\Pi = \{g(z) = 0\}$ for a C^1 smooth function g such that $\nabla g(z) \neq 0$.

The invariance of Π by the group generated by Γ_1 implies that, for $z \in \Pi$, $\langle J\nabla\Gamma_1(z)), \nabla g(z)\rangle = 0$ where J is the matrix of the standard symplectic form $dx \wedge dy$. In particular $\nabla g(z)$ belongs to the orthogonal subspace V_z to the vector $J\nabla\Gamma_1(z)$. One has $J\nabla\Gamma_1(z) = (x_2, -x_1, y_2, y_1)$ and its orthogonal subspace is generated by the vectors $\nabla\Gamma_2$, $\nabla\Gamma_3$ and $\nabla\Gamma_4$, where $\Gamma_4 = x_1y_1 + x_2y_2$.

But since $\langle X_0(z), \nabla\Gamma_2(z)\rangle = \langle X_0(z), \nabla\Gamma_3(z)\rangle = 0$, we conclude that the tranversality is lost at those points $z \in \mathbb{R}^4$ such that $\langle X_0(z), \nabla\Gamma_4(z)\rangle = 0$. This condition was analyzed before. From the previous discussion we conclude then that there exists $z \in \Pi \cap W^{u/s}(0)$ where the flow of X_0 is not transversal to Π. Since X coincides up to $\mathcal{O}(\delta^2)$ with X_0 the transversality condition to order δ is the same for both vector fields. □

Next we show the dynamics of the return map P_M to the section Π. Each initial condition is propagated by integrating (1) and, along the solution, Γ_3 is computed after transforming the coordinates by the change of coordinates generated by the Hamiltonian (21) that reduces the system to the Sokolskii NF up to order four.[2]

We display iterates of P_M in Fig. 18. From left to right, the three plots of the top row correspond to $\epsilon = -0.5, -0.45$ and -0.445, respectively. For better comparison of the results for different ϵ we display the results using y_1, y_2-coordinates scaled by the factor $\omega/\sqrt{\epsilon - \epsilon_c}$ (recall that $\epsilon_c = -4/9$ and $\omega = \sqrt{2/3}$). We clearly observe in the plots the singular lines due to non-transversality of the section since no points are obtained near them.

For reference, in the plots of the first row we also display the first crossing with Π of 1234 points taken equidistributed along a circle in the s_1, s_2-variables of small enough radius on the local invariant manifolds $W^u(0)$ and $W^s(0)$ around the origin (see definition of the variables in Section 3.1. Next iterates of those points under P_M turn around the origin almost filling up what resembles a circle. Indeed, as previously stated, for X_0 the intersection of the invariant manifolds with Π lie on a circle.

The plots of the second row of Fig. 18 are magnifications of those of the first one. The splitting of the stable/unstable invariant manifolds for $\epsilon = -0.5$ is seen in the first plot. The other two plots show magnifications of the plots of the first row for $\epsilon = -0.45$ and -0.445 respectively. We remark that the orbits have many iterates of P_M near $\{y_1 = y_2 = 0\}$ because, due to the non-integrability, orbits have many maxima of $y_1^2 + y_2^2$ near this set. However, the interest is near the invariant manifolds (and far from the singular lines where there is non-transversality). As expected, in the coordinates used in the plots, we recognize the limit circle (of radius ≈ 10.73) where the invariant manifolds of the integrable system intersect Π.

Finally, Fig. 19 shows the iterates for $\epsilon = -0.5$ (left) and $\epsilon = -0.45$ (right) displayed in coordinates $\theta = \arctan(y_2/y_1)$, $r^2 = 2\Gamma_3$ and Γ_1. We see the oscillations Γ_1 for the system (1). For $\epsilon = -0.445$ (not displayed) the oscillations of Γ_1 in the interior of the circle radius 10.73 are $\mathcal{O}(10^{-5})$. This decay of the range of the oscillations is a consequence of the fact that the formal

[2]Simulations using the change to NF up to order 6 and 8 do not reveal further details in the region of interest.

integral Γ_1 provides an adiabatic invariant that is better preserved for smaller values of $\epsilon - \epsilon_c$.

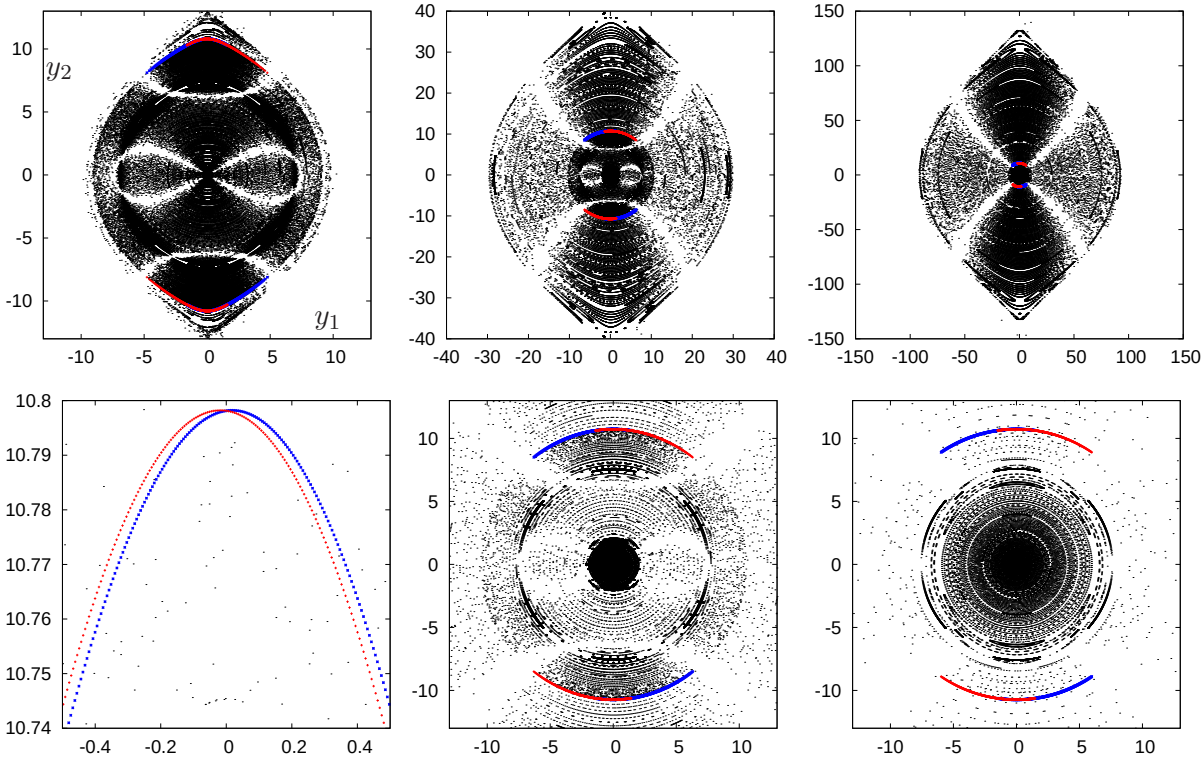

Figure 18: We display iterates of P_M for the same initial conditions and parameters considered to generate Fig. 8 and for $\epsilon = -0.5$ (left), -0.45 (center) and -0.445 (right). Also the first crossing of the invariant manifolds of the origin is shown. The second row plots are magnifications of the ones of the first row. The (y_1, y_2)-coordinates shown are scaled by the factor $\omega/\sqrt{\epsilon - \epsilon_c}$ to compare with Fig. 16.

D Investigation of the return times for the integrable system

We consider the truncation to order 4 of the Sokolskii NF reduction of the 2-DOF Hamiltonian-Hopf bifurcation given in (30) and, concretely, $H = -\Gamma_1 + \delta(\Gamma_2 - \Gamma_3 + \Gamma_3^2)$ where, for simplicity, suitable parameters of the unfolding have been chosen: we have considered $a = -1$ and $\eta = 1$ in the scaled Sokolskii NF (13). This is not restrictive since the rescaling $x_i \to (-\sqrt{\eta}a)x_i$, $y_i \to (-\sqrt{\eta}a)y_i$, $i = 1, 2$, $\delta \to \sqrt{-a}\delta$ reduces (30) to the case here considered. Below we report on the behavior of the return time as a function of the parameters (γ, h) for the nonlinear integrable flow of H to the Poincaré section Π, introduced in Appendix C, and to the section $\Sigma = \{\theta = 0\}$ used along the paper.

D.1 Return time to $\Pi = \{\max(y_1^2 + y_2^2)\}$

The pinched torus that form the invariant manifolds $W_H^u(0) = W_H^s(0)$ is a homoclinic surface inside the intersection of the 3D level sets $\{H = 0\}$ and $\{\Gamma_1 = 0\}$ that intersects $\Pi = \{\max(y_1^2 + y_2^2)\}$ transversally whenever $\Gamma_2 \neq \Gamma_3(2\Gamma_3 - 1)$, as shown in Appendix C. Hence, for $h_0, \gamma_0 > 0$

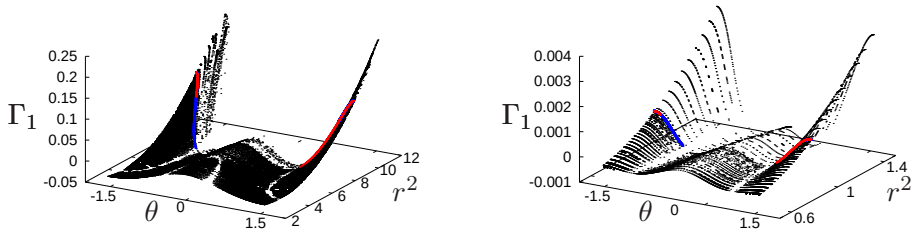

Figure 19: Iterates of P_M in coordinates θ, $2\Gamma_3$ and Γ_1 for $\epsilon = -0.5$ (left) and $\epsilon = -0.45$ (right). We observe the decay of the oscillations of Γ_1 as $\epsilon - \epsilon_c \to 0$ (that is, as getting closer to the Hamiltonian-Hopf bifurcation parameter). See text for details.

small enough

$$\hat{\Pi} = \{|H(z)| \leq h_0,\ |\Gamma_1(z)| \leq \gamma_0\} \cap \Pi \subset \mathbb{R}^4$$

defines a 3D section.

Selecting points on $\hat{\Pi}$ with h and γ given. Consider Γ_1 as a Hamiltonian and let $X_{\Gamma_1}(x,y) = (-x_2, x_1, -y_2, y_1)^\top$. We choose $q = (0,0,\sqrt{2},0) \in \{W^u_H(0) = W^s_H(0)\} \cap \{y_1^2 + y_2^2 = 2\}$, and we denote by $\mathcal{O}_{\Gamma_1}(q)$ its X_{Γ_1} orbit. One has

$$W^{u/s}_H(0) \cap \Pi = \mathcal{O}_{\Gamma_1}(q) = \{x_1 = x_2 = 0,\ y_1^2 + y_2^2 = 2\}.$$

Given $p \in \mathcal{O}_{\Gamma_1}(q)$ one has $X_H(p) = (\delta y_1, \delta y_2, -y_2, y_1)^\top$ and $X_{\Gamma_1}(p) = (0,0,-y_2,y_1)^\top$. Then,

$$\langle X_H(p), X_{\Gamma_1}(p)\rangle^\perp = \langle (0,0,y_1,y_2), (-y_2,y_1,0,0)\rangle =: \langle u_1, u_2\rangle.$$

Hence, given $p \in \mathcal{O}_{\Gamma_1}(q)$ and values h, γ, we look for a point

$$\tilde{p} = p + \alpha u_1 + \beta u_2 = (-\beta y_2, \beta y_1, (1+\alpha)y_1, (1+\alpha)y_2)$$

such that $H(\tilde{p}) = h$, $\Gamma_1(\tilde{p}) = \gamma$. One has $\Gamma_1(\tilde{p}) = 2\beta(1+\alpha)$, $\Gamma_2(\tilde{p}) = \beta^2$ and $\Gamma_3(\tilde{p}) = (1+\alpha)^2$, and the conditions to impose are

$$\Gamma_1(\tilde{p}) = 2\beta(1+\alpha) = \gamma, \qquad H(\tilde{p}) = \gamma + \delta(\beta^2 - (1+\alpha)^2 + (1+\alpha)^4) = h.$$

By substitution of $\beta = \gamma/(2(1+\alpha))$ into the condition for $H(\tilde{p})$ one obtains the equation

$$z^3 - z^2 - \left(\frac{\gamma + h}{\delta}\right) z + \frac{\gamma^2}{4} = 0, \qquad \text{where} \qquad z = (1+\alpha)^2.$$

Solving this equation for fixed values of h, γ and δ we obtain $\tilde{p}$ as required.

It remains to impose that the computed point belongs to Π. This can be done taking into account the next observations:

- If a point $z = (x,y) \in \Pi$ then $\Gamma_4(z) = x_1 y_1 + x_2 y_2 = 0$. One has $\Gamma_4(z) = \Gamma_4(w)$ for all $w \in \mathcal{O}_{\Gamma_1}(z)$.

- The points $p \in \mathcal{O}_{\Gamma_1}(q)$ are of the form $(0, 0, y_1, y_2)$, $y_1^2 + y_2^2 = 2$. Then $\Gamma_4(p) = 0$. On the other hand, $\tilde{p} = (-\beta y_2, \beta y_1, (1+\alpha)y_1, (1+\alpha)y_2)$ and $\Gamma_4(\tilde{p}) = 0$. In particular, for $p = q = (0, 0, \sqrt{2}, 0)$ one has $\tilde{q} = (0, \beta\sqrt{2}, (1+\alpha)\sqrt{2}, 0)$ and $\Gamma_4(\tilde{q}) = 0$. Moreover, the second order orbital derivative (32) of Γ_3 at $\tilde{q}$ is $-2\delta(1 + \mathcal{O}(\alpha, \beta^2))$, and it never vanishes for $|\alpha|$ and $|\beta|$ small enough. Then one has $\tilde{q} \in \Pi$.

It follows that $\mathcal{O}_{\Gamma_1}(\tilde{q}) \subset \Pi$. In the following, given h and γ, and for a fixed δ, we compute $\tilde{q}$ and we choose points in $\mathcal{O}_{\Gamma_1}(\tilde{q})$ as initial conditions on $\hat{\Pi} \cap \{H = h\} \cap \{\Gamma_1 = \gamma\}$ and we investigate the return time to $\hat{\Pi}$.

The return time to $\hat{\Pi}$. Once we know how to select initial points on Π we proceed to investigate the return time as a function of γ and h.

First, we introduce convenient variables to express the return map to Π. We recall that $\mathcal{O}_{\Gamma_1}(\tilde{q}) \in \Pi$ is the orbit of the point $\tilde{q}$ under the evolution given by the 4D linear system

$$\begin{pmatrix} \dot{x} \\ \dot{y} \end{pmatrix} = A \begin{pmatrix} x \\ y \end{pmatrix}, \quad \text{where} \quad A = \begin{pmatrix} J^\top & 0 \\ 0 & J^\top \end{pmatrix}, \quad J = \begin{pmatrix} 0 & 1 \\ -1 & 0 \end{pmatrix}.$$

Hence, we parameterize $\mathcal{O}_{\Gamma_1}(\tilde{q}) \subset \Pi$ by a parameter s so that

$$\mathcal{O}_{\Gamma_1}(\tilde{q}) = \{(x, y) \in \mathbb{R}^2 \times \mathbb{R}^2, (x, y)^\top = \exp(As)\tilde{q}^\top, s \in [0, 2\pi)\},$$

and, in particular, $\mathcal{O}_{\Gamma_1}(q) = \{(x, y) \in \mathbb{R}^2 \times \mathbb{R}^2, x = 0, y = \sqrt{2}(\cos(s), \sin(s)), s \in [0, 2\pi)\}$.

Then, we express the return map to Π for the vector field X_H in terms of coordinates (h, γ, t, s), where t is the time of the system evolution. For the integrable system one has

$$(h, \gamma, t, s) \to (h, \gamma, t + t_v(h, \gamma, s), s + s_v(h, \gamma, s)).$$

Numerical evidence supports that t_v and s_v only depend on h and γ, that is $t_v(h, \gamma, s) = t_v(h, \gamma)$ and $s_v(h, \gamma, s) = s_v(h, \gamma)$. The results on the behavior of t_v as a function of h and γ are summarized in Fig. 20. The hyperbolic point is located at the level of energy $h = 0$ and the corresponding time t_v displays the typical logarithmic behavior as a function of the action Γ_1. This is shown in the third of the bottom plots of Fig. 20. For other energy levels the time t_v remains finite. We observe that it shows maxima for Γ_1 close to h.

As the time evolves from $t = 0$ to $t = t_v$ a given initial point in Π with parameter s returns to Π at a different point on $\mathcal{O}_{\Gamma_1}(\tilde{q})$ corresponding to $s + s_v(h, \gamma)$. One expects s_v to be related to t_v in some way. Let us consider first the energy $h = 0$. In Fig. 21 left we display $t_v(0, \gamma)$ and $s_v(0, \gamma)$ (since $s_v \in [0, 2\pi)$ we display $s_v + 55$ to see better the relation between s_v and t_v). Note that for $h = 0$ we expect $t_v \sim \log(\gamma)/\delta + b$, for some constant b, since at this level of energy one has the hyperbolic point. The lack of symmetry of t_v in the figure indicates that for $\gamma > 0$ and $\gamma < 0$ different values of b are expected. On the other hand, one checks from computations that

$$s_v(0, \gamma) = \begin{cases} t_v(0, \gamma) + \delta - 2\pi[t_v(0, \gamma) + \delta/(2\pi)], & \gamma > 0, \\ t_v(0, \gamma) + \delta + \pi - 2\pi[t_v(0, \gamma) + \delta + \pi/(2\pi)], & \gamma < 0. \end{cases} \tag{33}$$

For $h \neq 0$ the relation between t_v and s_v is not so evident. Both are displayed in Fig. 21 for $h = 0.005$. To better compare them, in Fig. 21 right we show the behavior of s_v and t_v near the maxima. In particular, the maxima do not coincide and are reached for different values of γ close to, but to the left of, $\gamma = h$.

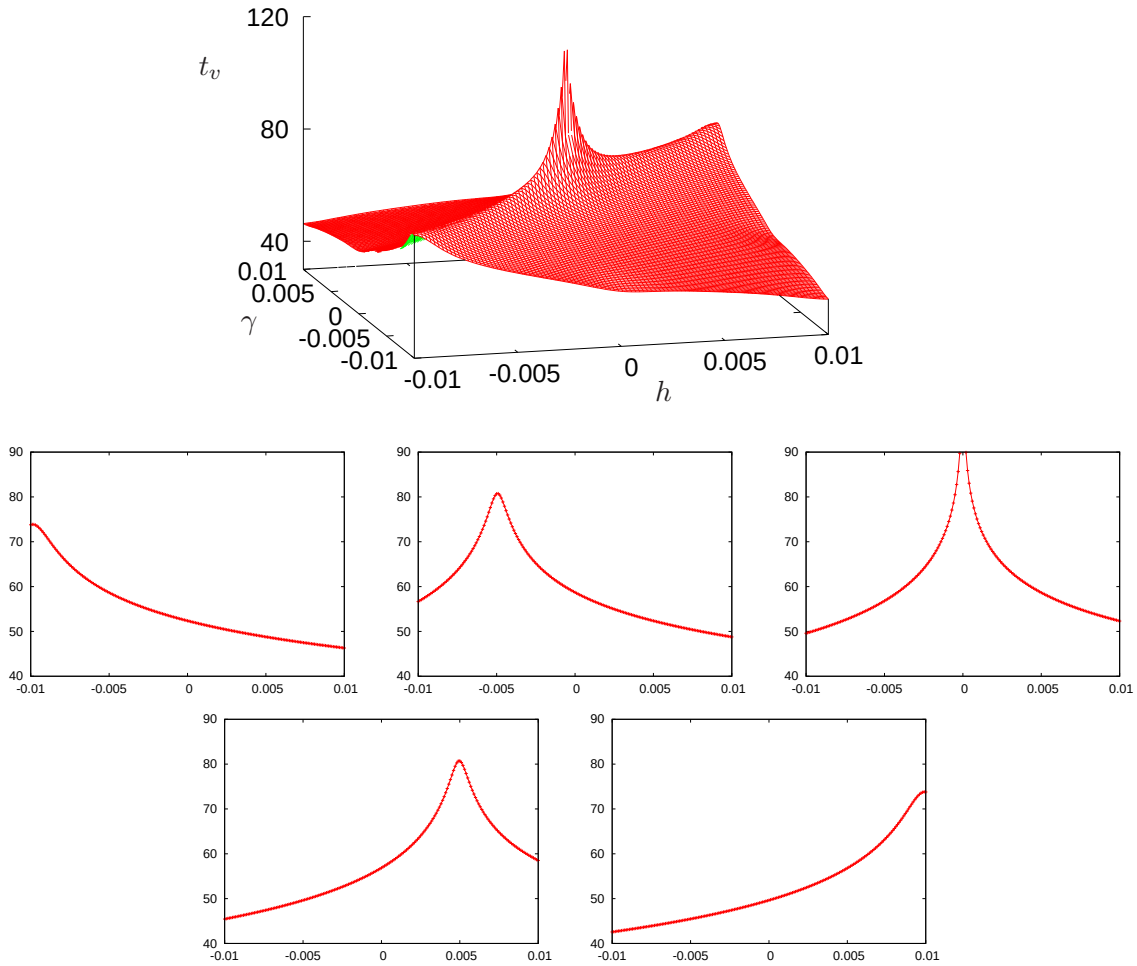

Figure 20: Return time t_v as a function of h and γ. The bottom plots display t_v as a function of γ for the values of $h = -0.01(0.005)0.01$ (from left to right). The value of $\delta = 0.1$ has been selected for these illustrations.

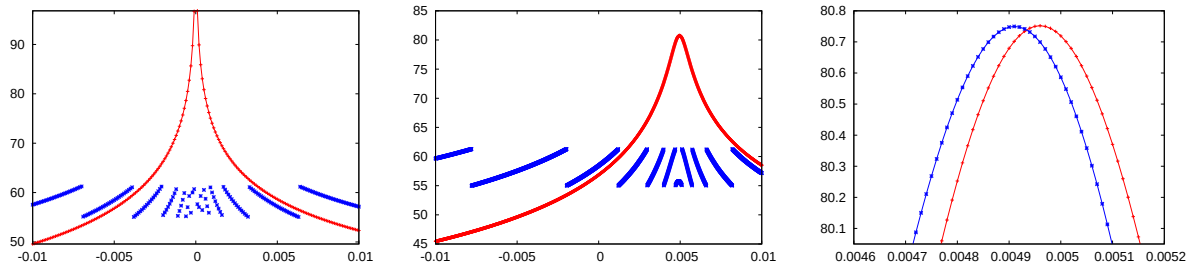

Figure 21: We display the return time t_v together with $s_v + 55$ as a function of γ for $h = 0$ in the left plot and for $h = 0.005$ in the center one. Also for $h = 0.005$, in the rightmost plot we display $s_v + 79.98$ and t_v as a function of γ near their maxima. We see that maxima are not reached for $\gamma = h$ but for close different values of γ. As before $\delta = 0.1$ in all plots.

D.2 Return time to a fundamental domain FD in $\Sigma = \{\theta = 0\}$

Now we choose $\Sigma = \{\theta = 0\}$ as a return section. Expressed as a function of the Cartesian coordinates $\Sigma = \{g(y_1, y_2) := \arctan(y_2/y_1) = 0\}$, then $X_H(z)\nabla g(z) = 1 - \delta\Gamma_1/r^2$ and the section is transversal for $r \approx \sqrt{\delta}$, distance up to which the invariant manifolds extend, provided Γ_1 is small enough. That is, for $\gamma_0,\ h_0 > 0$ small enough,

$$\hat{\Sigma} = \{|H(z)| \leq h_0,\ |\Gamma_1(z)| \leq \gamma_0\} \cap \Sigma \subset \mathbb{R}^4$$

defines a 3D transversal section that we shall use to construct the return map.

We recall from Section 4.1 that the invariant manifolds of H in Σ form a loop as the one that possesses the Duffing system. In order to capture just one point of each orbit we simply consider iterates in Σ near $s = \arctan(x_1/y_1) = 0$ as follows.

1. Given a point $z = (x_1, x_2, y_1, 0) \in \Sigma$ we consider $h = H(z)$, $\gamma = \Gamma_1(z)$ and $s = S(z) := \arctan(x_1/y_1)$ as coordinates to identify such a point.
2. The solution of the Cauchy problem associated to X_H with initial condition $p_0 = (h, \gamma, 0)$ intersects $\Sigma = \{\theta = 0\}$ several times. We restrict to crossings such that $y_1 > 1/2$ and we consider p_1 to be the first crossing with Σ with $s > 0$.
3. Let $s_1 = S(p_1)$, note that $s_1 = s_1(h, \gamma)$. The set $\texttt{FD} = \{(h, \gamma, s) \in \Sigma, |h| \leq h_0, |\gamma| \leq \gamma_0, s \in [0, s_1)$ defines a fundamental domain. This is analogous to the fundamental domain FD introduced in Section 6.1.
4. The return map P is defined as follows: Given $p = (h, \gamma, s)$ with $s \in [0, s_1)$ we define $q = P(p)$ as the first crossing of the solution with initial condition p such that $S(q) > 0$ and $y_1(q) > 1/2$ with Σ.

Return time to FD. We investigate the return time to the fundamental domain for the integrable system H for a fixed $\delta > 0$. To this end, we choose initial conditions on FD as follows: a point $(h, \gamma, s) \in \texttt{FD}$ identifies an initial condition of the form $(\sqrt{z}\tan(s), \gamma/\sqrt{z}, \sqrt{z}, 0)$ where z is the solution nearest to 2 of the equation

$$\frac{z^3}{2} + (\tan^2(s) - 1)z^2 - 2\frac{(\gamma + h)}{\delta}z + \gamma^2 = 0.$$

We are interested in values of $|\gamma| \approx 0$, then the existence of such solution requires $\gamma + h = \mathcal{O}(\delta)$. The range of γ in experiments need to be adjusted accordingly (depending on δ).

Then we compute the image under the return map to FD as described above. In Fig. 22 left we illustrate the return time for the set of points of the form $(h, \gamma, 0)$ for $h, \gamma = -0.01(10^{-4})0.01$. We see that as $h, \gamma \to 0$ the return time tends to infinity in a logarithmic way while rotating around the asymptote at $h = \gamma = 0$. On Fig. 22 right we display the s coordinate of the image of these points as a function of h and γ.

References

[1] V. I. Arnol'd. *Mathematical methods of classical mechanics*. Springer-Verlag, New York-Heidelberg, 1978. Translated from the Russian by K. Vogtmann and A. Weinstein, Graduate Texts in Mathematics, 60.

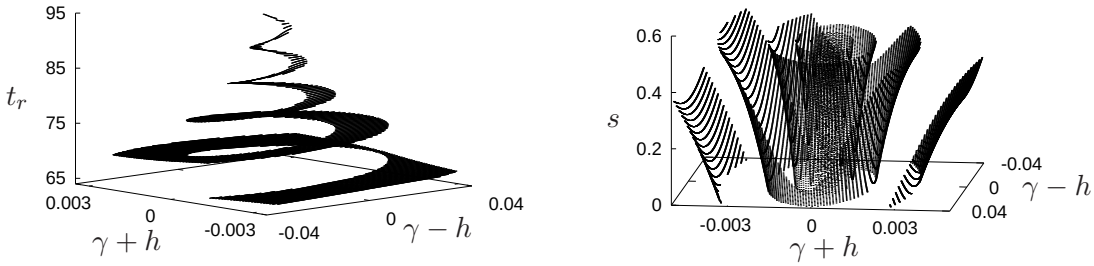

Figure 22: For both plots we consider $\delta = 0.1$ and the same set of initial conditions with $s = 0$ in FD. Left: We display the return time t_r to FD as a function of $h, \gamma \in [-0.01, 0.01]$. Right: We display the coordinate s after one return to FD.

[2] C. Batut, K. Belabas, D. Bernardi, H. Cohen, and M. Olivier. *Users' guide to PARI/GP*. http://pari.math.u-bordeaux.fr/.

[3] H. Broer, C. Simó, and J.C. Tatjer. Towards global models near homoclinic tangencies of dissipative diffeomorphisms. *Nonlinearity*, 11:667 – 770, 1998.

[4] N. Burgoyne and R. Cushman. Normal forms for real linear Hamiltonian systems with purely imaginary eigenvalues. *Celestial Mechanics and Dynamical Astronomy*, 8(4):435–443, 1974.

[5] X. Cabré, E. Fontich, and R. de la Llave. The parameterization method for invariant manifolds. III. Overview and applications. *J. Differential Equations*, 218(2):444–515, 2005.

[6] B.V. Chirikov. A universal instability of many-dimensional oscillator system. *Phys. Rep.*, 52:264 – 379, 1979.

[7] A. Delshams and T.M. Seara. Splitting of separatrices in Hamiltonian systems with one and a half degrees of freedom. *Math. Phys. Electron. J.*, 3:Paper 4, 40, 1997.

[8] J.C. Van der Meer. *The Hamiltonian Hopf Bifurcation*. Lecture Notes in Mathematics, 1160. Springer-Verlag, 1985.

[9] R.L. Devaney. Homoclinic orbits in Hamiltonian systems. *J. Differential Equations*, 21(2):431–438, 1976.

[10] J.J. Duistermaat. The monodromy in the Hamiltonian Hopf bifurcation. *Z. Angew. Math. Phys.*, 49(1):156–161, 1998.

[11] H. Eliasson. *Hamiltonian systems with Poisson commuting integrals*. PhD thesis, Univ. of Stockholm, 1984.

[12] S. Ferraz-Mello. Periodic Orbits in a Region of Instability Created by Independent Small Divisors. In P.E. Nacozy and S. Ferraz-Mello, editors, *Natural and Artificial Satellite Motion, Proceedings of the International Symposium held at University of Texas at Austin, 1977*, pages 283–292. University of Texas Press, 1979.

[13] B. Fiedler. Real chaos and complex time. Talk given at the Annual International Conference on Dynamical Systems "Shilnikov Workshop", Lobachevsky University of Nizhny Novgorod (Russia), 2021.

[14] E. Fontich. Rapidly Forced Planar Vector Fields and Splitting of Separatrices. *Journal of Differential Equations*, 119(2):310 – 335, 1995.

[15] E. Fontich and C. Simó. The Splitting of Separatrices for Analytic Diffeomorphisms. *Ergod. Th. and Dynam. Sys.*, 10:295–318, 1990.

[16] E. Fontich, C. Simó, and A. Vieiro. On the "hidden" harmonics associated to best approximants due to quasi-periodicity in splitting phenomena. *Regular and Chaotic Dynamics*, 23(6):638–653, 2018.

[17] E. Fontich, C. Simó, and A. Vieiro. Splitting of the separatrices after a Hamiltonian-Hopf bifurcation under periodic forcing. *Nonlinearity*, 33(4):1440–1493, 2019.

[18] J.P. Gaivão and V. Gelfreich. Splitting of separatrices for the Hamiltonian-Hopf bifurcation with the Swift-Hohenberg equation as an example. *Nonlinearity*, 24(3):677–698, 2011.

[19] V. Gelfreich. Near strongly resonant periodic orbits in a Hamiltonian system. In *Proceedings of the National Academy of Sciences USA*, number 22 in 99, pages 13975–13979, 2002.

[20] V. Gelfreich, C. Simó, and A. Vieiro. Dynamics of 4D symplectic maps near a double resonance. *Physica D*, 243(1):92–110, 2013.

[21] V.G. Gelfreich and V.F. Lazutkin. Splitting of separatrices: perturbation theory and exponential smallness. *Russian Math. Surveys*, 56(3):499–558, 2001.

[22] V.G. Gelfreich, V.F. Lazutkin, and M.B. Tabanov. Exponentially small splittings in Hamiltonian systems. *Chaos*, 1(2):137–142, 1991.

[23] V.G. Gelfreich and C. Simó. High-precision computations of divergent asymptotic series and homoclinic phenomena. *Discrete Contin. Dyn. Syst. Ser. B*, 10(2-3):511–536, 2008.

[24] H. Hanßmann. *Local and semi-local bifurcations in Hamiltonian dynamical systems: Results and examples*. Lecture Notes in Mathematics, 1893. Springer-Verlag, 2007.

[25] À. Haro, M. Canadell, J-Ll. Figueras, A. Luque, and J.M. Mondelo. *The parameterization method for invariant manifolds*, volume 195 of *Applied Mathematical Sciences*. Springer, [Cham], 2016. From rigorous results to effective computations.

[26] M.H.C.F. Lacaz. Stability in the double resonance problem. *Celestial Mechanics*, 35:9–17, 1985.

[27] L. M. Lerman and Ya. L. Umanskiy. *Four-dimensional integrable Hamiltonian systems with simple singular points (topological aspects)*, volume 176 of *Translations of Mathematical Monographs*. American Mathematical Society, Providence, RI, 1998. Translated from the Russian manuscript by A. Kononenko and A. Semenovich.

[28] L.M. Lerman and Ya.L. Umanskiĭ. Classification of four-dimensional integrable hamiltonian systems and poisson actions of $\mathbb{R}^2$ in extended neighborhoods of simple singular points. I. *Russian Acad. Sci. Sb. Math.*, 77:511–542, 1994.

[29] K.R. Meyer and G. Hall. *Introduction to Hamiltonian dynamical systems and the N-body problem*. Applied Mathematical Sciences, 90. Springer-Verlag, New York, 1992.

[30] J. Moser. The Analytic Invariant of an Area-Preserving Mapping Near a Hyperbolic Fixed Point. *Comm. Pure Appl. Math.*, IX:673 – 692, 1956.

[31] A. Neishtadt. The separation of motions in systems with rapidly rotating phase. *Prikladnaja Matematika i Mekhanika*, 48:133–139, 1984.

[32] T.Z. Nguyen. A note on focus-focus singularities. *Differential Geom. Appl.*, 7(2):123–130, 1997.

[33] Á. Pelayo and S. Vũ Ngọc. Symplectic theory of completely integrable Hamiltonian systems. *Bull. Amer. Math. Soc. (N.S.)*, 48(3):409–455, 2011.

[34] G.N. Piftankin and D.V. Treschev. Separatrix maps in Hamiltonian systems. *Russian Math. Surveys IOP*, 2(62):219–322, 2007.

[35] H. Rüssmann. Über das Verhalten analytischer Hamiltonscher Differentialgleichungen in der Nähe einer Gleichgewichtslösung. *Math. Ann.*, 154:285–300, 1964.

[36] C. Simó and A. Vieiro. Resonant zones, inner and outer splittings in generic and low order resonances of area preserving maps. *Nonlinearity*, 22(5):1191–1245, 2009.

[37] C. Simó and A. Vieiro. Dynamics in chaotic zones of area preserving maps: close to separatrix and global instability zones. *Physica D*, 240(8):732–753, 2011.

[38] C. Simó and A. Vieiro. Some remarks on the abundance of stable periodic orbits inside homoclinic lobes. *Physica D: Nonlinear Phenomena*, 240(24):1936–1953, 2011.

[39] A.G. Sokolskiĭ. On the stability of an autonomous Hamiltonian system with two degrees of freedom in the case of equal frequencies. *J. Appl. Math. Mech.*, 38:741–749, 1974. Translated from Prikl. Mat. Meh. 38, 791–799 (Russian), 1974.

[40] J. Stöber and A. Bäcker. Geometry of complex instability and escape in four-dimensional symplectic maps. *Phys. Rev. E*, 103(4):042208–, 2021.

[41] J. Williamson. On the Algebraic Problem Concerning the Normal Forms of Linear Dynamical Systems. *Amer. J. Math.*, 58(1):141–163, 1936.

[42] G.M. Zaslavskiĭ, M.Y. Zakharov, R.Z. Sagdeev, D.A. Usikov, and A.A. Chernikov. Stochastic web and diffusion of particles in a magnetic field. *Zh. Èksper. Teoret. Fiz.*, 91(2):500–516, 1986.

[43] G.M. Zaslavsky and N.N. Filonenko. Stochastic instability of trapped particles and conditions of applicability of the quasi-linear approximation. *Soviet Physics JETP*, 27:851–857, 1968.

[44] M. Zou. Monodromy in two degrees of freedom integrable systems. *J. Geom. Phys.*, 10(1):37–45, 1992.